JNC TN9400 2001−122

Simulation of the MIXA-06 Experiment by SIMMER-Ⅲ

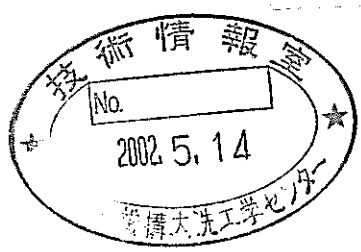

June, 2001

O-ARAI ENGINEERING CENTER
JAPAN NUCLEAR CYCLE DEVELOPMENT INSTITUTE

Ⓚ

JNC TN9400 2001 – 122
June 2001

Simulation of the MIXA-06 Experiment by SIMMER-III

Xuewu CAO*, Yoshiharu TOBITA*

Abstract

MIXA-06 experiment performed at Winfrith Technology Centre in which 3 kg of molten fuel simulant (81% uranium dioxide and 19% molybdenum metal at a temperature of 3600 K) were released into water is selected to estimate the fragmentation model in SIMMER-III code on the mixing region in the case of low Weber numbers in this study. The comparison of the front advancement of the melt droplet stream between the simulation and the experiment suggests that the currently employed hydrodynamic fragmentation model in SIMMER-III underestimates the fragmentation rate of the droplets in the simulation with low Weber numbers. The further investigation shows the fragmentation model based on the thermal fragmentation mechanism is required.

* Nuclear system Safety Research Group, Advanced Technology Division, (former System Engineering Technology Division), O-arai Engineering Center, JNC

SIMMER-III によってMIXA-06 の実験のシミュレーション

（研究報告）

曹　学武*、飛田　吉春*

要　旨

Winfrith Technology Centre で行われた MIXA-06 の実験では３ｋｇの溶融燃料模擬物質(3600K の 81% 二酸化ウランと 19% モリブデン 金属の混合物質) を水に落下させ、FCI の粗混合過程が研究されている。この実験のシミュレーションを通じて、SIMMER-III の FCI の溶融粒子細粒化に関わるモデルの検証を行う。溶融粒子集団のフロントの位置を実験結果と比較したところ、hydrodynamic 溶融粒子細粒化モデルは粒子の水中での落下速度を低 Weber 数の場合に過大に評価するため、 thermal 溶融粒子細粒化メカニズムを考慮した溶融粒子細粒化モデルが必要とされることが分かった。

* 大洗工学センター　要素技術開発部　リスク評価研究グループ

Contents

List of figures

List of tables

1. Introduction

Fuel Coolant Interactions (FCIs) are the important phenomena in nuclear reactor severe accident analysis, which have been numerically studied in recent years. Several mathematical models have been developed to study the premixing phase of FCIs. The SIMMER-III code is one of them, developed in JNC [1,2]. The mixing region, which is expressed as the front advancement of the melt droplet stream in this study, is dominated by the drag coefficient (Cd) between the droplets and coolant liquid, the surface area (A_d) of the droplets and the heat transfer from the droplets to the coolant liquid. Since the drag coefficient (Cd) model for the hot droplet with vapor film moving in coolant liquid was estimated through the simulation of the QUEOS experiment [3,4] by the SIMMER-III code in the previous study [5,6], and the heat transfer coefficient was estimated in the previous study [7], the difference of the front advancement of the melt droplet stream between the simulated and the experimental results is mainly affected by the surface area (A_d) model, which is related to the fragmentation model of the droplets, suggesting that it is essential to numerically study the FCI process.

Previous studies [8,9] showed that in high Weber number case, hydrodynamic mechanism dominates the fragmentation process, but under the condition of the low Weber numbers, thermal fragmentation mechanism may dominate the fragmentation process, caused by the vapor film collapse or the surface solidification of the melt droplets. For example, Matsumura [10] experimentally study the self-triggering vapor explosions by using tin-water system. The results show that in a certain range of temperatures of the melt droplet and coolant the thermal fragmentation mechanism dominates the fragmentation of the droplets. Cronenberg [11,12] and Corradini [9] studied the influence of the surface solidification of the melt droplets and concluded that the influence of the surface solidification should be accounted for the case with a high melting point of the melt droplets. Although the thermal fragmentation mechanism induced by the self-triggering event has been studied many years, the fragmentation rate model for simulation tools induced by the self-triggering event has not been searched.

In the current SIMMER-III code, the hydrodynamic fragmentation model (Taylor type correlation and Pilch and Erdman's correlation) [1,2] is employed, which is developed based on the relative velocity between the droplets and coolant liquid. In this study, the validity of the fragmentation model employed in the SIMMER-III code is tested and

evaluated through the simulation of the MIXA experiment [13] in the study of the FCI process under the condition of low Weber numbers.

2. Description of experiment

MIXA are the simulant experiments of the mixing study of FCIs, which were performed at Winfrith Technology Centre [13]. The experimental facility is shown in Fig. 1, involved the release of several kilograms of molten fuel simulant (81% uranium dioxide and 19% molybdenum metal at a temperature of 3600 K) into the pool of water. A droplet former is employed to ensure that the melt enters the water as a stream of droplets with a diameter of approximately 6 mm. The skirt is attached beneath the droplet former to control the radial spreading of the stream of the droplets. The experimental vessel is of square section with a side of 0.37 m and a pool depth of 0.6 m. The vessel is left open to the atmosphere via a venting line, which contains a flow-meter to measure the steam produced as the melt droplets enter the water. The initial pressure is 0.1 MPa in the experiment and the water is initially heated to near the saturated temperature.

In the MIX-06 experiment a central pour of 3 kg of melt droplets in the form of approximate 6 mm diameter droplets is produced. When the melt droplets are released from the melt generator, the droplet stream of 120 mm in diameter is produced by the cylindrical skirt. The melt droplets pour lasts for a total time of 1.0 s. The main data in the MIXA06 experiment are summarized in table 1.

3. SIMMER-III Representation

3.1 Geometry, initial conditions and calculation system

The MIXA experimental vessel, which is the square-section vessel, as shown in Fig. 1, is modeled as an axis-symmetric cylindrical volume with the same cross sectional area as the real vessel in a diameter of 0.42m and a total height of 1.5 m with a depth of 0.6 m region, which consists of a water pool, and 0.9 m region below the melt generator filled with the air, open to outside, as shown in Fig. 2. A constant pressure boundary condition is employed at the exit. The melt droplets flow into the vessel through the hole with a diameter of 0.12 m in the center on the vessel top. The stream of the melt droplets with a volume fraction of 0.05 flows into the vessel at a rate of 3 kg/s in a time interval of 1.0 second.

For all calculations, an initial melt droplet size of 6 mm is specified, which is

consistent with the value in the experiment. The material of the melt droplets in the experiment is the mixture of 81% uranium dioxide and 19% molybdenum metal at a temperature of 3600 K, which is simulated by 100 % uranium dioxide with the same temperature. The free gas space is initially filled with the air with initial pressure 0.1 MPa and temperature 371 K. Since the vessel is open to the outside, the composite of gas does not have much influence on the calculated results. The temperature of water in the vessel is 371 K. The main data used in the simulations are summarized in table 2.

The geometric model, shown in Fig. 2, is discretized radially by 10 nodes with Δr=0.021 m and axially by 40 nodes with Δz=0.0375 m. The calculations are carried out with a time step of $\Delta t = 4 \times 10^{-4}$. The initial radii of the melt droplets are set to 0.003 m. The minimum radius of the melt droplets is set to 0.001 m to correspond average diameter of the droplets of 0.002 m estimated after the experiment. The Taylor correlation (hydrodynamic fragmentation model) is employed to model the fragmentation of the droplets with the fragments of 0.002 m. 0.0001 m, 0.000001 m and 0.0001 m are set for the initial, minimum and maximum radii of water respectively. The modified ILUBCG method is selected for fluid dynamics algorithm. The orifices plate is set in the flow-out cell in the calculation domain in order to simulate the venting system in the experiment. The multipliers of the drag coefficient among dispersed components and between dispersed and continuous components are set to 1.0 (default value) respectively. The continuous inflow/outflow is set to the boundary cell in the open exit on the top of the domain, in which the pressure is set to constant of 0.1 MPa. The calculation is started from the time of –0.38 second in order to make that the contact time of the melt droplets with water is 0.0 second.

3.2 Input data set

The input data for the reference calculation is listed in Appendix A.

3.3 Code version and computer used

Calculations are based on SIMMER-III Version 2.F (ALPHA, DBL, URANAS options on). The computer used was an EWS ALPHA.

3.4 Code modifications

No code modifications.

3.5 Parametric cases

In order to estimate the influence of the fragmentation model on the mixing region, the following cases are carried out based on the base case described in section 3.1. The differences between these cases and the base case are listed in the following for each case.

Cases 1: The fragmentation of the droplets is modeled by setting the same value of the minimum and maximum radii of the melt droplets in the mixing region in this case, which means that when the droplets enter the water region, they are immediately fragmented into small parts with a diameter of 0.002 m.

Case 2: The Taylor correlation is employed to model the fragmentation of the droplets with the fragments of 0.001 m (0.002 m in base case).

Case 3: The difference between this case and the base case is that the time constant multiplier for the Weber breakup of the melt droplets in the bubbly region (CFSB) and the time constant multiplier for the Weber breakup of the melt droplets in the dispersed region (CFSD) is set to 0.001 (1.0 in base case) to investigate the influence of the fragmentation time in Taylor correlation on the mixing region.

Case 4: The maximum and minimum radii of the melt droplets are set to the initial value of 0.003 m in the mixing region, which means no fragmentation of the droplets. This case is designed to understand the influence of the current fragmentation model on the mixing region by obtaining the difference of the front advancement of the droplet stream induced by the current fragmentation model between two cases.

Case 5: This case is designed to understand the difference between the Pilch and Erdman's correlation [14] for the fragmentation of the droplets and the Taylor correlation in the base case.

Cases 6 and 7: The critical Weber number is set to 0.12. The CFSB and CFSD are set to 1.0 and 0.001 respectively to understand which parameters in the Taylor type correlation for the fragmentation of the droplets affect the fragmentation rate.

Case 8 and 9: The fragmentation model of the melt droplets is specified by setting the same value of the minimum and maximum radii of the melt droplets in mixing region, as in case1. The minimum radius of the droplets is set to 0.0015 and 0.0007 m respectively in the two cases to obtain the influence of the size of the fragmented droplets on the mixing region.

4. Results and discussion

4.1 Base case

The calculated results of the base case include the front advancement of the stream of the melt droplets (the expression of the mixing region), the pressure transient, the steam flow rate, the cumulative steam volume vented and water level swell, summarized in the following.

The front advancements of the stream of the melt droplets in water both in the simulation and the experiment are plotted in Fig. 3, which shows that the calculated penetration rate of the stream of the droplets is faster than that measured from the experiment. Since the front advancement of the droplet stream is dominated by the drag coefficient between the droplets and coolant liquid, the heat transfer coefficient and the surface area of the droplets, in which the drag coefficient and the heat transfer coefficient were estimated in the previous studies [5,6,7], the difference of the front advancement of the droplet stream between the simulated and the experimental results is mainly resulted from the surface area model, which is related to the fragmentation rate of the droplets. The current fragmentation model employed in the base case is the Taylor correlation (hydrodynamic fragmentation model). The calculated results show that the fragmentation rate of the droplets is underestimated. (The underestimation of the surface area of the droplets causes the faster penetration in the water. The simulated result of MIXA01 experiment also suggests this conclusion, as shown in Fig. 19.)

The calculated and measured pressure transients in the free gas space in the vessel are plotted in Fig. 4, which shows that the predicted pressure transient is larger than that observed in the experiment during the penetration of the droplet stream in the water (from 0 to 0.5 second), although the penetration velocity is much faster than the experiment, which can be explained by the overestimation of the heat transfer coefficient from the droplets to the water.

The transient steam production rate can be compared with the code output, as shown in Fig. 5. The experimental data show that the steaming rate increases steadily from zero to a peak of about 1.0 m^3/s over a period of 0.7 s. But the calculated results give a high steam production rate at the beginning and lower rate after 0.6 second, which is in accordance with the pressure transient. Integration of the measured steam flow rate shows that in the experiment approximately 0.5 m^3 of steam escaped from the vessel in 1.0

second after the melt droplet stream entered water region. The calculated cumulative steam volume is recorded and plotted in Fig. 6, which shows that the calculated steam loss is a little lower than that measured in the experiment. The steam production suggests that the fragmentation rate of the droplets is underestimated by employing the Taylor correlation.

The calculated water level swell is shown in Fig. 7, which is much higher than that measured from the experiment. The higher water level is thought to be caused by the measurement method. In the calculation, the highest point in the head of the gas chimney wall is measured as the water level. In the experiment the water level at the corner may be measured as the water level, which is much lower than that in the head of the gas chimney wall . In the base case the 10% water fraction contour is taken to represent the water level.

The distribution of the droplet size could not be obtained from the calculation. In the base case the radius of the fragments is set to 0.001 m, but it can not be known that during the penetration, whether or not the size of the fragments reaches the value. In the following the cases are calculated to investigate the influence of the parameters on the mixing region, which is related to the fragmentation model.

4.2 Sensitivity calculations

In case 1, the fragmentation of the droplets is modeled by setting the values of the minimum and maximum radii of the melt droplets to 0.001 m in the mixing region, which means that when the droplets enter the water region, they are immediately fragmented into small parts with a diameter of 0.002 m. The front advancements of the stream of the melt droplets in water both in the simulation and the experiment are plotted in Fig. 8, which shows that the calculated penetration rate of the stream of the droplets is slower than that measured from the experiment and the base case. The result of this case shows that the fragmentation rate of the droplets is overestimated by using such fragmentation model. The real fragmentation rate of the droplets in the experiment is that between the base case and this case, which is supported by the calculated results of the pressure transient, the steam flow rate, the cumulative steam volume vented in this case (fragmentation rate of the droplets is overestimated), which are shown in Figs. 9, 10, 11 respectively.

In case 2 the Taylor correlation is employed to model the fragmentation of the droplets, but the minimum diameter of the fragments is set to 0.001 m instead of 0.002 m in the base case. The front advancements of the stream of the melt droplets in water both in this case and the base case are plotted in Fig. 12, which suggests that the calculated

penetration rates of the stream of the droplets are almost the same in both cases. The calculated results suggest that during the penetration, the diameter of most of the fragments does not reach the average value of 0.002 m as estimated from the experiment, which means the Taylor correlation fragmentation model underestimates the fragmentation rate in the simulation of the experiment.

The case 3 is designed to investigate the influence of the fragmentation time in Taylor correlation on the mixing region. The difference is that CFSB and CFSD are set to 0.001 in this case instead of 1.0 in the base case. The front advancement of the stream of the melt droplets is shown in Fig. 13. Although the fragmentation time is set to very small, the front advancement does not changed so much in these two cases, which show this parameter does not work in the calculation of these cases.

Then, the case 4 is designed to understand the influence of the current fragmentation model on the mixing region by obtaining the difference of the front advancement of the droplet stream induced by the current fragmentation model between two cases. The maximum and minimum radii of the melt droplets are set to the initial value, which means no fragmentation in this case. The front advancement of the stream of the melt droplets is plotted in Fig. 14, which shows that in this case the front advancement of the melt droplets is faster than those both in the experiment and in the base case. These calculated results suggest that the currently employed fragmentation model works in the simulation of the experiment, but the fragmentation rate is underestimated.

The case 5 is designed to understand the difference between the Pilch and Erdman's correlation [14] for the fragmentation of the droplets (implemented in SIMMER-III) and the Taylor correlation in the base case. The front advancement of the droplet stream is plotted in Fig. 15, showing no difference by using these two fragmentation models, which are hydrodynamic fragmentation models.

In the cases 6 and 7, the critical Weber number is set to 0.12. The CFSB and CFSD are set to 1.0 and 0.001 respectively to understand which parameters in the Taylor type correlation for the fragmentation of the droplets affect the fragmentation rate. The front advancement of the droplets are plotted in Fig. 16, which shows that when the critical Weber number is set to 12, even though the fragmentation time is set to very small (in case 3), the front advancement of the melt droplets is not changed, but when the critical Weber number is set to 0.12 and fragmentation time is reduced 1000 time, the penetration rate is

much reduced, as shown in the result of case 7. These calculated results suggest that the critical Weber number and the fragmentation time are the factors affecting the fragmentation rate in the simulation of the experiment. The calculation shows that in the experiment, the Weber number of the droplets in the system is around or less than 12, which means part of the fragmentation process of the droplets during the penetration is cut off, inducing low fragmentation rate in the calculation. These results suggest that under the condition of low Weber numbers the hydrodynamic fragmentation model could not describe the fragmentation rate of the melt droplets.

In case 8 and 9 the fragmentation model of the melt droplets is specified by setting the same value of the minimum and maximum radii of the melt droplets in mixing region, as in the case1. The minimum radius of the droplets is set to 0.0015 and 0.0007 m respectively in the two cases to obtain the influence of the size of the fragmented droplets on the mixing region. The front advancement of the melt plotted in Fig. 17, which shows that the front advancement is sensitive to the minimum radius of the melt droplets.

4.3 Fragmentation Mechanism

4.3.1 Currently Used Fragmentation Model in SIMMER-III

The calculated results of MIXA-06 experiment show that the currently used fragmentation model in SIMMER-III [1,2] underestimates the fragmentation rate of the droplets, in which the interfacial area (A_d) between the droplets and the coolant can be described by

$$\frac{\partial A_d}{\partial t} + \nabla \bullet (v A_d) = \sum_k S_d . \qquad (1)$$

The source term (S_d) of the interfacial area of the droplets is modeled by the following correlation:

$$S_d = \frac{A_d^e - A_d}{\tau_d}, \qquad (2)$$

where τ_d is time interval, the equilibrium interfacial area A_d^e is calculated by the equilibrium radius r_d^e and the volume fraction α_d of droplets:

$$A_d^e = \frac{3\alpha}{r_d^e}. \qquad (3)$$

The equilibrium radius is assumed to be the maximum stable size of the droplets governed by the hydrodynamic stability criterion related to a critical Weber number:

$$r_d^e = \frac{We_{Cr}\sigma}{2\rho_c \Delta v^2}, \tag{4}$$

where Δv is the relative velocity difference between continuous and dispersed phases, ρ_c is the continuous phase density and the critical Weber number We_{Cr} is 12.

The time interval is calculated by

$$t_b^* = \frac{\Delta v \varepsilon^{0.5}}{2r_d}\tau_d, \tag{5}$$

where ε is the density ratio of the continuous dispersed phases and for liquid-liquid system t_b^* is given as

$$t_b^* = 13.7Bo^{-0.25}. \tag{6}$$

where

$$Bo = \frac{3}{8}C_d\frac{\rho r_d \Delta v^2}{\sigma} \tag{7}$$

These equations show that the fragmentation rate is related to the relative velocity between the droplets and the coolant liquid. The calculated results show that the currently employed fragmentation model underestimated the fragmentation rate in the simulation of the MIXA-06 experiment, under the condition of the low Weber numbers. That the critical Weber number has a big effect on the fragmentation of the droplets suggests that the fragmentation mechanism should be studied, before the fragmentation rate model is selected.

4.3.2 Possible Fragmentation Mechanism in FCI

Corradini [9] reviewed the theory and modeling in vapor explosion and summarized that the fragmentation mechanisms are categorized into two classes hydrodynamic and thermal effects. The hydrodynamic fragmentation occurs when a melt droplet is subjected to external surface forces sufficient to overcome the droplet surface tension. There are several kinds of hydrodynamic fragmentation mechanisms; Rayleigh-Taylor instability,

Kelvin-Helmholtz instability and boundary layer stripping. If two different fluids having a common boundary are accelerated in the direction from the lighter liquid to the heavier liquid perpendicular to the boundary, the irregularities of the interface will tend to grow, which is Rayleigh-Taylor instability. If the two fluids have a relative velocity, the perturbation of the interface also will tend to grow, which is Kelvin-Helmholtz. In boundary layer stripping, the tangential components of flow at the droplet surface exert a shearing force, which sets the layer at the edge of the droplet, i.e. the boundary layer detaches itself and breaks up into a fine mist of droplets.

Thermal fragmentation mechanisms include boiling effects, internal pressurization and solidification effects. When the melt droplet is introduced into the cold liquid, a vapor film is formed to surround it. The collapse of the vapor film causes the fragmentation of the droplet. The behavior of the vapor film is related to the temperatures of the droplet and coolant, ambient pressure and properties of the coolant and the droplet. If the temperature of the melt droplet decreases from film boiling temperature to nucleate temperature of the coolant, it undergoes a quenching process. The unstable heat transfer across the vapor film from film boiling to nucleate boiling causes the vapor film unstable and collapse, inducing the droplet fragmentation. Even if the temperature is very high and the film boiling is stable, the collapse of the vapor film can be caused by strong triggering event, which causes liquid-liquid contact and generates local high pressure. The collapse of the vapor film may cause the coolant jets entrapment into the droplet and evaporation of the coolant jets break the droplet into small parts, as described by Kim [15]. The internally generated pressures cause the breakup of the surrounding development of thermal stresses in the melt droplet. When the resultant thermal stress is greater than the yielding stress of the material, fissures may develop in the outer frozen shell, inducing the breakup of the droplet [16].

4.3.3 Fragmentation Mechanism in High Melting Point FCI

The investigation suggests that the thermal fragmentation mechanism has contribution to the fragmentation of the melt droplets in the MIXA-06 experiment. Thermal effects include boiling effects, internal pressurization and solidification effects, which are believed to have relation with the collapse of the vapor film. In MIXA-06 what is the correct mechanism for fragmentation of the melt droplets? When the melt droplets are released into water, a vapor film is formed to surround the melt droplet, as shown in Nelson's experiment [17]. Because the temperature of the melt droplets in MIXA-06 is very high

(3600 K), the vapor film is stable. Since no strong pressure pulse (triggering event) is applied in the vessel, the stable vapor film collapse induced by pressure pulse is not considered to be the dominant triggering event. Self-triggering vapor film collapse is the possible explanation for fragmentation. Since the volume fraction of the melt droplets is very small, about 0.05 and no pressure peak was recorded in the experiment, quenching is the possible reason for the fragmentation of the droplets.

As shown in Fig. 18, the quenching process can be explained by the boiling curve. As the temperature of the melt droplets decreases to point D, the heat transfer rate decreases. At point D the vapor film becomes unstable and collapses toward the surface of the melt droplets. The melt droplets are above the boiling point of the coolant and the vapor film is re-established. In this transition region, coolant periodically contacts the heating surface. The transition can be very violent and continuous until the nucleate boiling regime is attained at point C. When the temperature difference between the droplet and water is reduced to about 140 K, the boiling enter transition region, which maybe induce the breakup of the melt droplets.

In order to check the boiling effect, it should be known that the temperature change during the penetration of the melt droplets into water in MIXA-06.Tthe following equation can be used to describe the temperature change of the melt droplet.

$$mc_p \frac{dT}{dt} = -hA(T - T_s) \tag{8}$$

where m is the mass of the melt droplet, T is the temperature of the melt droplet, A is the surface of the melt droplet, h is the heat transfer coefficient from the melt droplet to coolant, T_s is the temperature of the coolant. Then temperature transient of the droplet can be obtained as

$$\frac{T - T_s}{T_m - T_s} = e^{\frac{-3h}{\rho c_p r}t} \tag{9}$$

Here the heat transfer coefficient from the melt droplet to water at film boiling is about 10^5 to 10^6 $W/(m^2K)$. The temperature T_s of water is about 373 K. When the melt droplet with a radius of 0.003 m is cooled from 3600 K to 140 K (freezing is not considered), it takes about 0.005 to 0.05 second, which is less than the time of 0.4 second

that the melt droplets take to arrive the vessel bottom. Although the boiling effect can be the triggering event in the experiment, the solidification point of UO2 is about 3100 K, which is much larger than 400K. This means that the solidification effect is much more possible than the boiling effect. The surface temperature reaches the melting point much earlier than the estimated value (less than 0.001 to 0.01 second). When the surface temperature becomes lower than the melting point, the outer part of the melt droplet becomes solid. The analysis suggests that the freezing-provoked droplet fragmentation mechanism may be the dominant fragmentation mechanism in the MIXA-06 experiment.

In the experimental analysis, most of the debris was in the form of irregular globules, giving the impression of frozen droplets before they arrived the bottom of the vessel. These droplets, which ranged in size from fine power (<0.1 mm) to 10 mm, had a shiny, polished appearance. The nature of the debris strengthen the analysis that freezing-provoked droplet fragmentation mechanism may be the dominant fragmentation mechanism in the MIXA-06 experiment.

5. Conclusions

The hydrodynamic fragmentation model employed in the SIMMER-III code is estimated under the condition of low Weber numbers through the simulation of the MIXA-01 and 06 experiments. The calculated results show that the currently employed hydrodynamic fragmentation model in the SIMMER-III code underestimates the surface area of the droplets in the simulation of the experiment with low Weber numbers. The investigation suggests that the fragmentation model of the melt droplets based on the thermal fragmentation mechanism is required to be developed. The freezing-provoked droplet fragmentation mechanism (thermal fragmentation) is considered to be the dominant mechanism to increase surface area of the droplets in the experiment, which is not taken into account in the current SIMMER-III model.

6. Recommendations for model improvements

Based on the calculated results, the thermal fragmentation model is recommended to be developed for the SIMMER-III code.

Acknowledgements

The authors wish to express their thanks to Dr. H. Niwa of O-arai Engineering Center, JNC for his useful discussions.

Nomenclature

English Symbols

A surface area of droplets (m^2)

Bo instantaneous Bond number ($Bo = \frac{3}{8} C_d \frac{\rho r_d \Delta v^2}{\sigma}$)

C_d drag coefficient

D diameter (m)

h heat transfer coefficient

m mass

P pressure (Pa)

r radius (m)

S interfacial area source term

t time

T temperature

v velocity (m/s)

We Weber number ($We = \frac{\rho_c D \Delta v^2}{\sigma}$)

Greece Symbols

α volume fraction of the droplet

ε density ratio

δ thickness of vapor film (m)

μ viscosity ($Pa \cdot s$).

ρ density (kg/m^3).

σ surface tension of the droplet

τ time interval

Subscripts and superscripts:

c coolant, continuous phase

cr criticality

d droplet

e equilibrium quantity

References

(1) Sa. Kondo, D.J.Brear, Y.Tobita, K.Morita, W.Maschek, P.Coste and D.Wilhelm, Status and Achievement of Assessment Program for SIMMER-III, a Multiphase, Multicomponent Code for LMFR Safety Analysis, Proceedings of Eighth International Topical Meeting on Nuclear Reactor Thermal-Hydraulics, Vol. 3, Kyoto, Japan, Sept. 30-Oct. 4 1997

(2) K.Morita, Sa.Kondo, Y.Tobita and D.J.Brear, SIMMER-III Application to Fuel-Coolant Interactions, Proceedings of the OECD/CSNI Specialists Meeting on Fuel- Coolant Interactions May 19-21, 1997, Tokai-mura, Japan.

(3) L.Meyer, QUEOS, an Experimental Investigation of the Premixing Phase with Hot Spheres, Proceedings of Eighth International Topical Meeting on Nuclear Reactor Thermal-Hydraulics, Vol. 3, Kyoto, Japan, Sept. 30-Oct. 4 1997

(4) L.Meyer, G.Schumacher, QUEOS, a Simulation-Experiment of the Premixing Phase of a Steam Explosion with Hot Spheres in Water Base Case Experiments, FZKA Report 5612, Forschungszentrum Karlsruhe, April 1996.

(5) X. Cao and Y. Tobita, Simulation of Premixing Experiment QUEOS by SIMMER-III, JNC TN9401 2000-100 (2000).

(6) X. Cao, and Y. Tobita, A Drag Correlation for a Hot Particle/Droplet with vapor film, (in submission to J. of Nuclear Science and Technology)

(7) D.Brear, A Guide to Heat Transfer Coefficients in SIMMER-III Version 2.d, PNC ZN9410 98-026, April 1998

(8) G.Berthoud, F.Crecy, R.Meignen, Description of Premixing with the MC3D Code including molten jet behavior modeling. Comparison with FARO Experiment results. Proceedings of the OECD/CSNI Specialists Meeting on Fuel- Coolant Interactions May 19-21, 1997, Tokai-mura, Japan.

(9) M. L. Corradini, B. J. Kim and M. D. OH, Vapor explosions in light water reactors: a review of theory and modeling, Progress in Nuclear Energy, Vol. 22, No. 1. pp. 1-117, 1988

(10) K. Matsumura, et al, Thermal Interaction Zone and Self-triggering Mechanism of Tin-Water Systems, The international seminar on Intense Multiphase Interactions, June 9-13,1995, Santa Barbara.

(11) A.W.Cronenberg,T.C.Chawla and H.K. Fauske, A thermal stress mechanism for the fragmentation of Molten UO2 upon contact with sodium coolant, Nuclear Eng. Des. 30 (1974) 434-443.

(12) A.W.Cronenberg,M.A.Grolmest, Fragmentation Modeling Relative to the Breakup of Molten UO2 in Sodium, Nuclear Safety, Vol, 16, No. 6, 1975.

(13) M.K.Denham, A.P.Tyler and D.F.Fletcher, Experiments of The Mixing of Molten Uranium Dioxode with Water and Initial Comparision with CHYMES code Calculations, NURETH-5, Salt Lake City, UT, 1992, pp. 1667-1675.

(14) M.Pilch and C. Erdman, Use of breakup time data and velocity history data to predict the maximum size of stable fragments for acceleration-induced breakup of a liquid drop, Int. J. Multiphase Vol. 13, No. 6, pp.741-757, 1987.

(15) B. Kim and M. L.Corradini, Modeling of small-scale single droplet fuel/coolant interactions, Nuclear Science and Engineering, Vol. 98, 16-28 (1988)

(16) W. Zyszkowski, Thermal interaction of molten copper with water, Int. J. Heat Mass Transfer, Vol. 18, No. 2, pp. 271-287, 1975.

(17) L.S.Nelson, P.M.Duda, Steam Explosion Experiments with Single Drops of Iron Oxide Melted with a CO2 Laser Part II. Parametric Studies, NUREG/CR-2718, SAND82-1105, 1985.

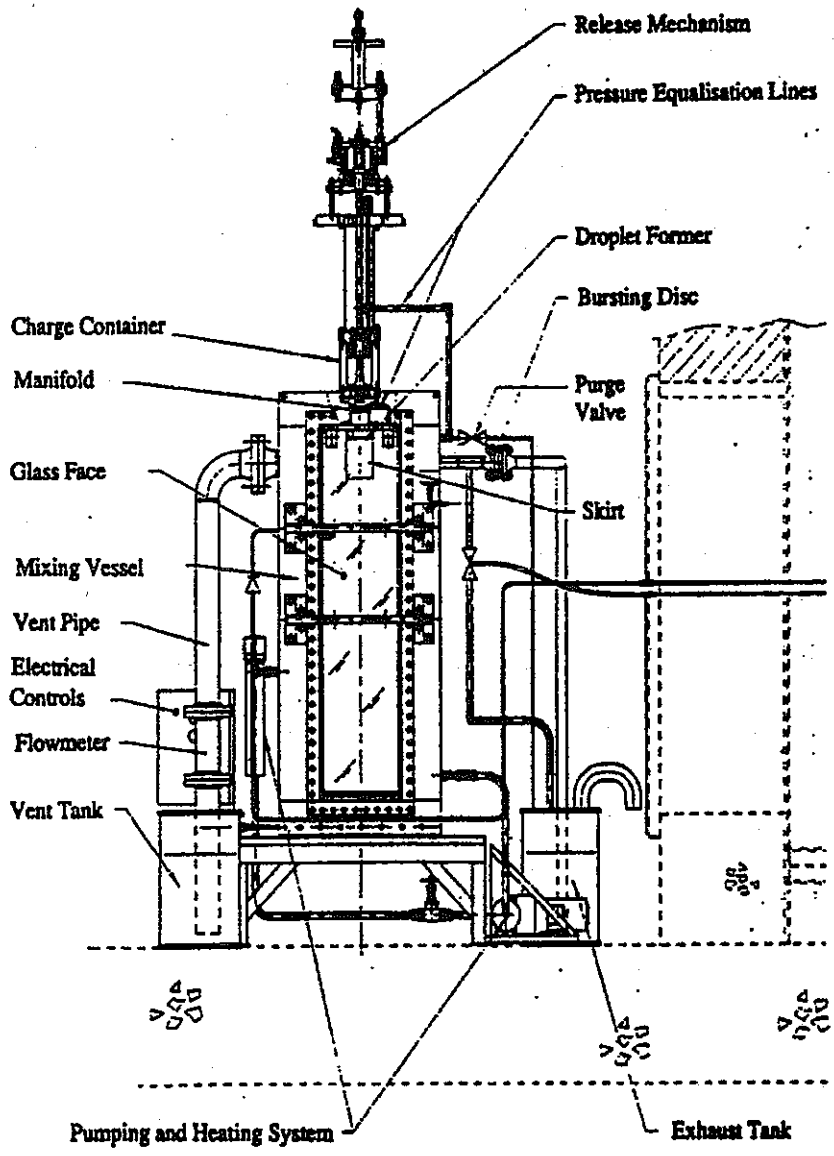

Fig. 1 Scheme of the MIXA facility

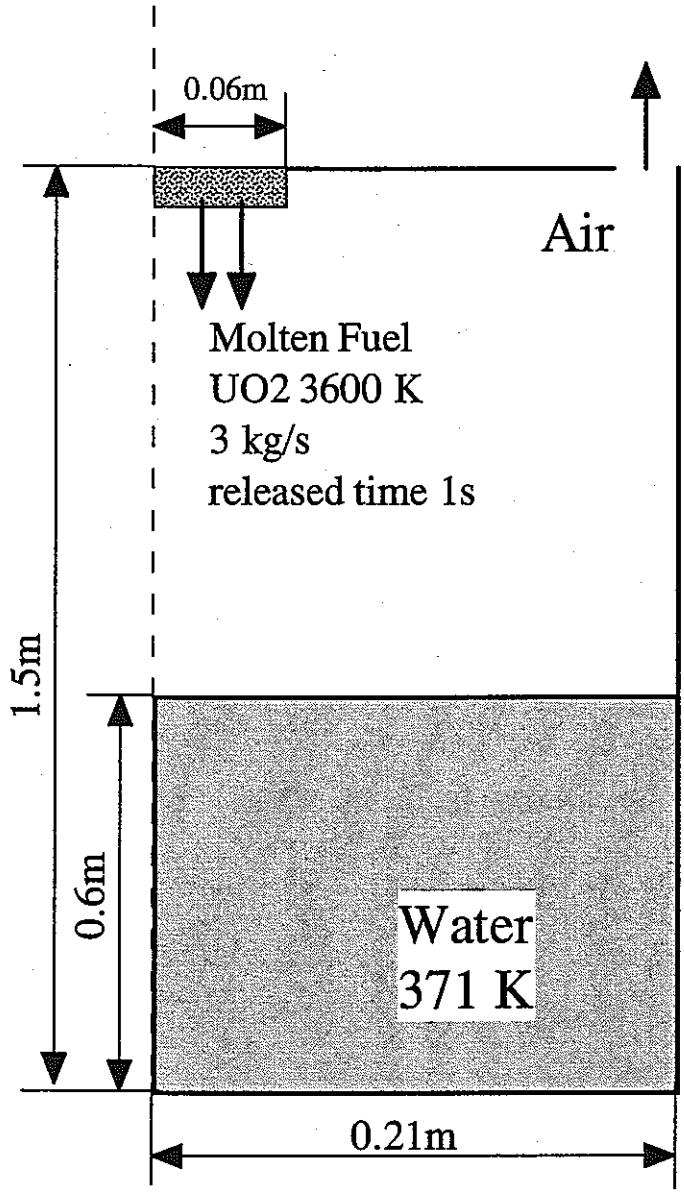

Fig. 2 The computational domain used in the MIXA-06 simulation

Table 1 Data of the experiment MIXA-06

Experimental No.	MIXA-06
Molten Material	UO2 81% + Molybdenum 19%
Initial diameter of drops (mm)	6
Mass of drops released (kg)	3
Initial temperature of drops (K)	3600
Initial radius of melt droplets stream (m)	0.06
Density of spheres (g/cm3)	8.4
Drops volume fraction at the impact on the water	0.05
Time for first spheres enter water (Sec)	0.0
Water Vessel	
Cross section	37x37 cmxcm
Height (cm)	150
Water level (cm)	60
Water temperature (K)	Near saturated
Pressure loss coefficient of venting pipe	1.0

Table 2 Data used for the simulation of MIXA-06

Simulation No.	MIXA-06
Melt droplet Material	UO2
Initial diameter of melt droplets (mm)	6
Mass of melt droplets (kg)	3
Initial temperature of melt droplets (K)	3600
Initial velocity of melt droplets stream (m/s)	0.7
Initial volume fraction of melt droplets	0.05
Initial radius of melt droplets stream (m)	0.06
Water vessel	Cylindrical geometry
Radius (m)	0.21
Height (cm)	1.5
Water level (m)	0.6
Pressure loss coefficient of vent pipe	1.0
Initial pressure in vessel (Pa)	1E5
Temperature of water in vessel (K)	371.0
Temperature of air in gas space (K)	371.0
Time	
Calculation start time (Sec)	-0.38
Real time at cal. Start time (Sec)	-0.38

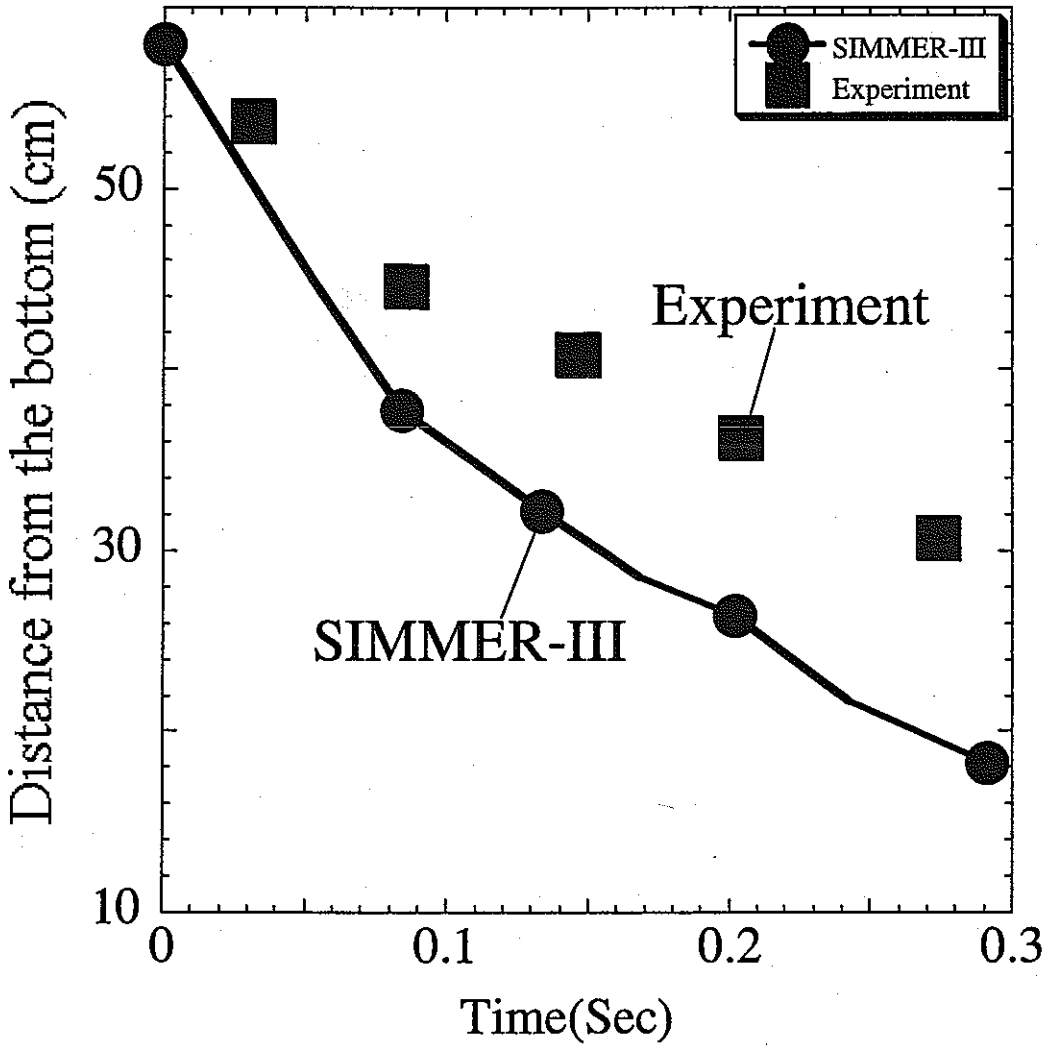

Fig. 3 Front advancement of the droplet stream in water in the experiment and the simulation (base case) of MIXA-06.

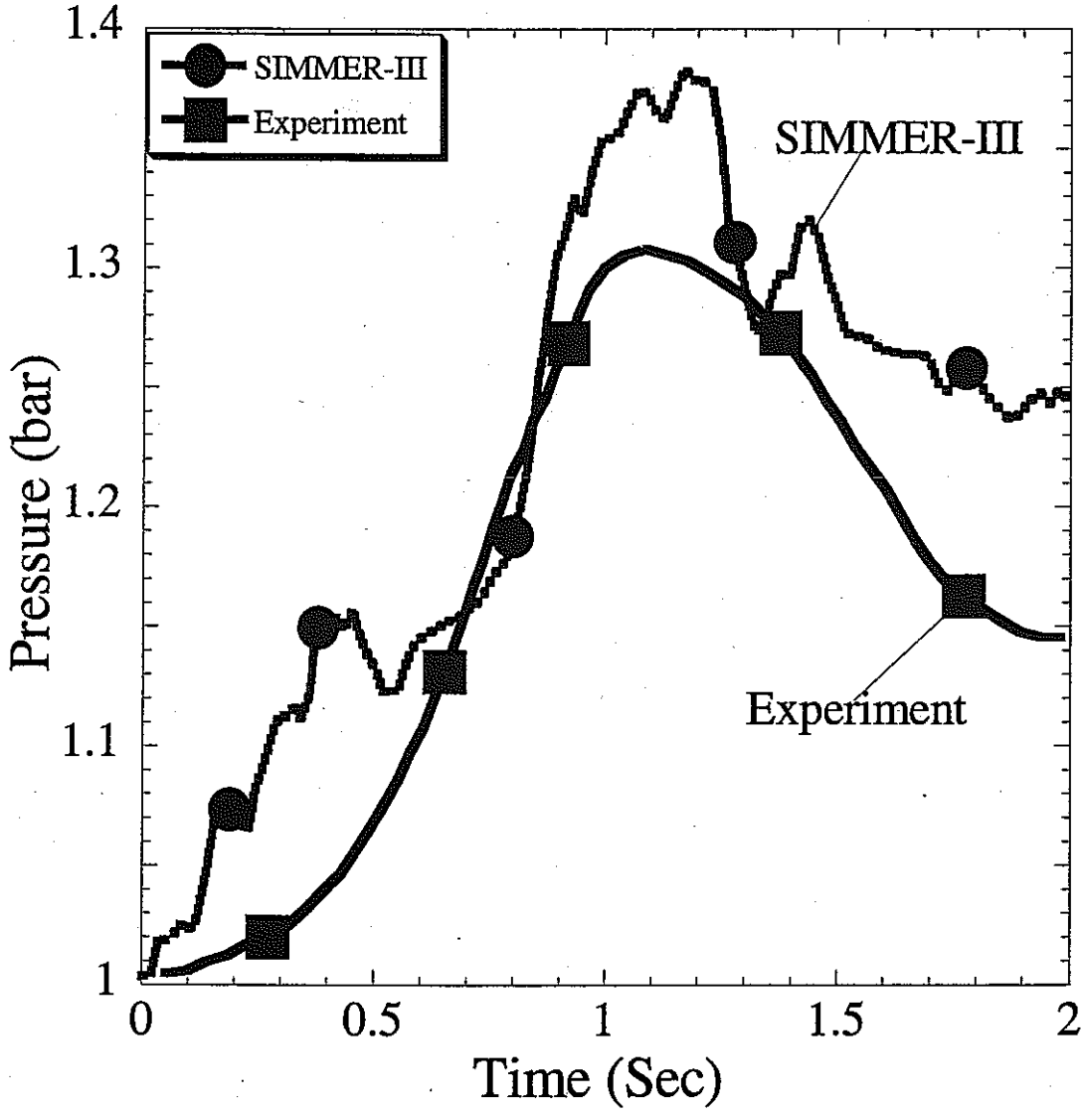

Fig. 4 The pressure transient in the free gas space in the experiment and the simulation (base case) of MIXA-06.

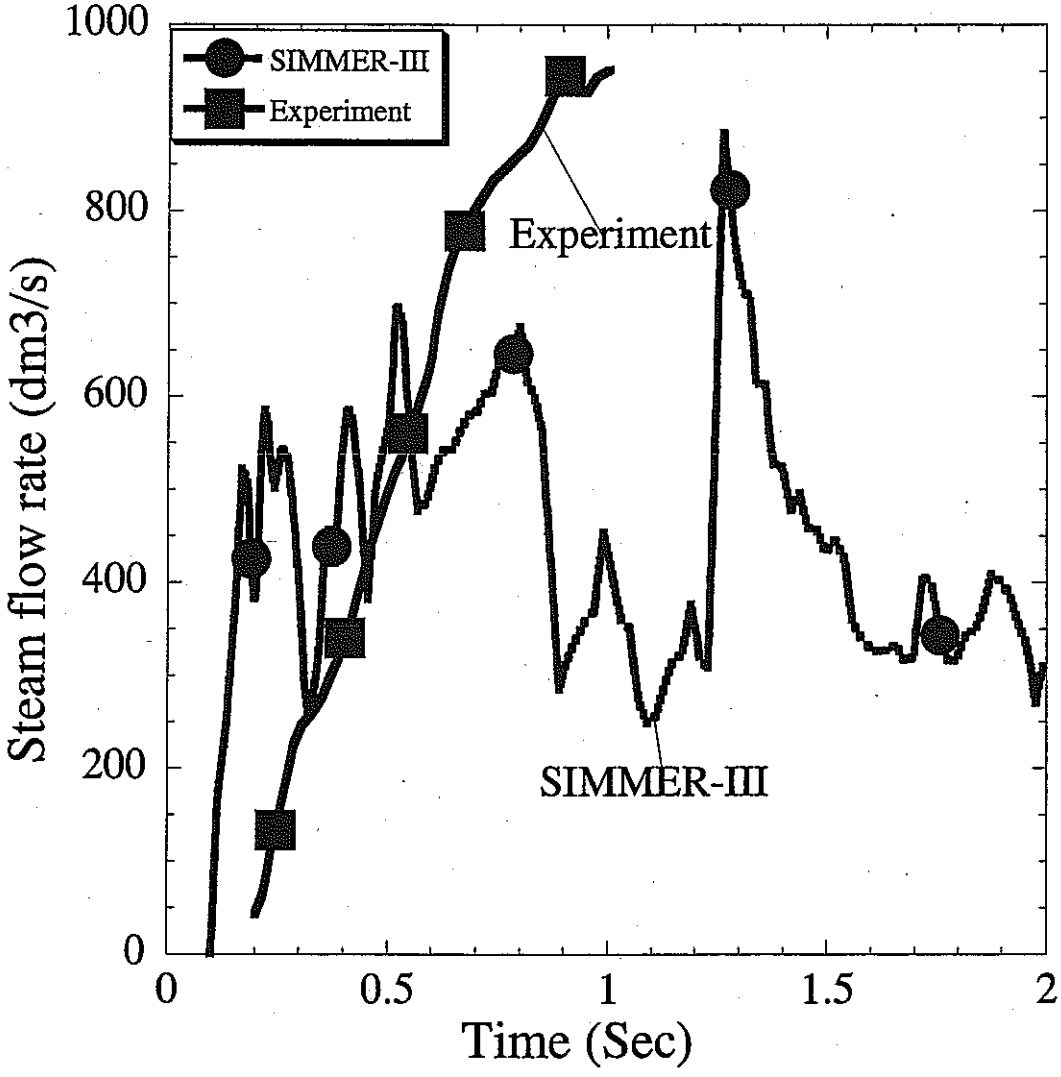

Fig. 5 Steam flow rate in the experiment and the simulation (base case) of MIXA-06.

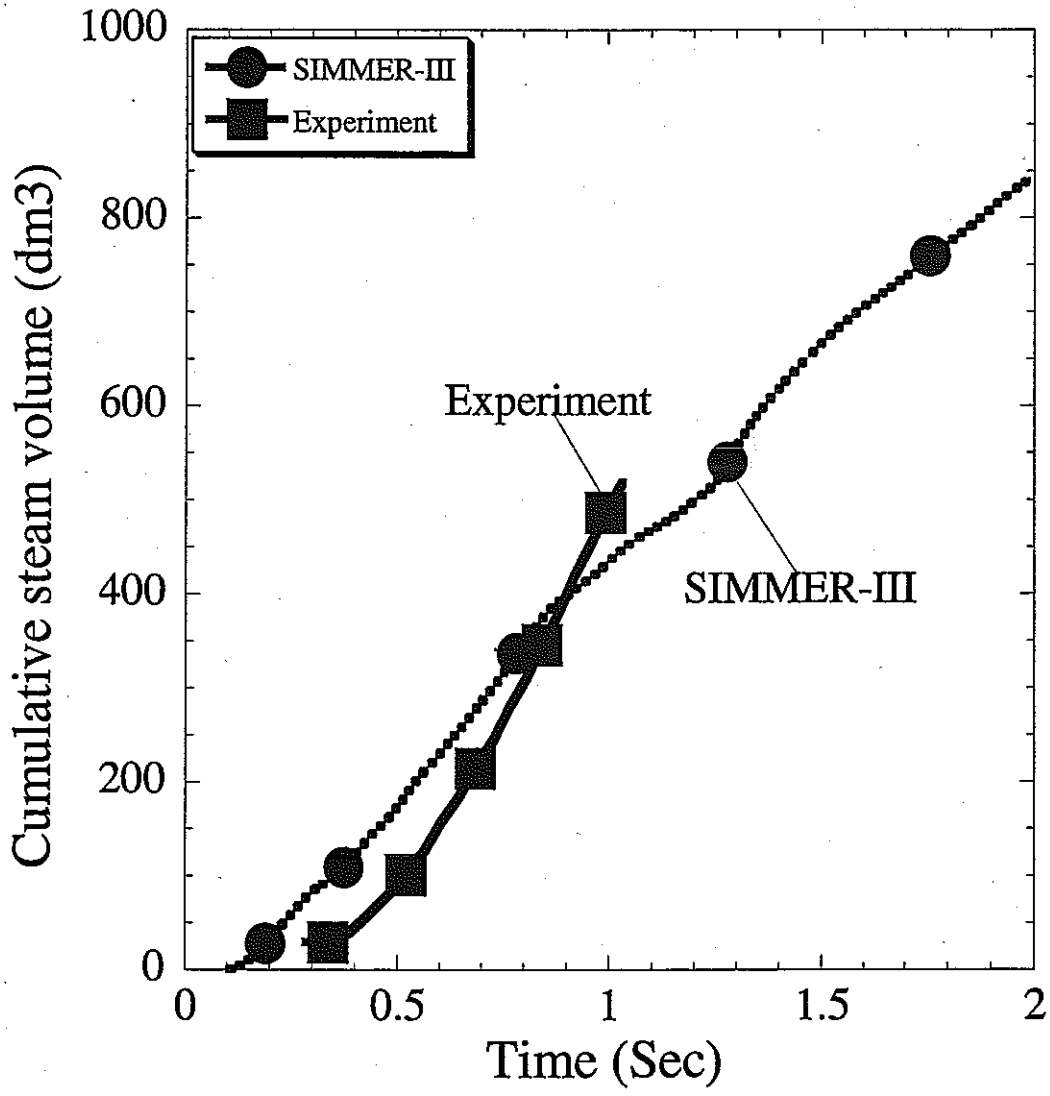

Fig. 6 Cumulative steam volume in the experiment and the simulation (base case) of MIXA-06.

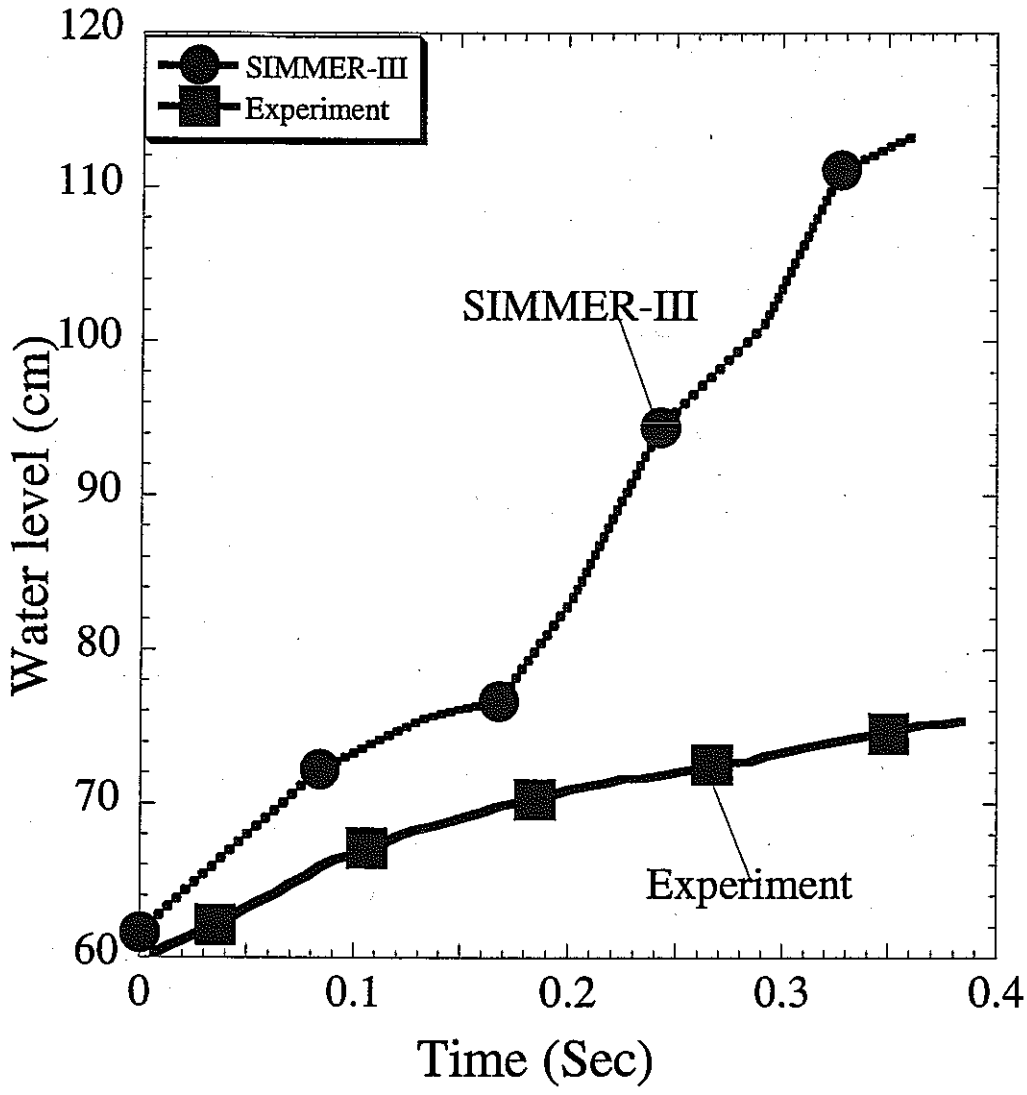

Fig. 7 Water level swell in the experiment and the simulation (base case) of MIXA-06.

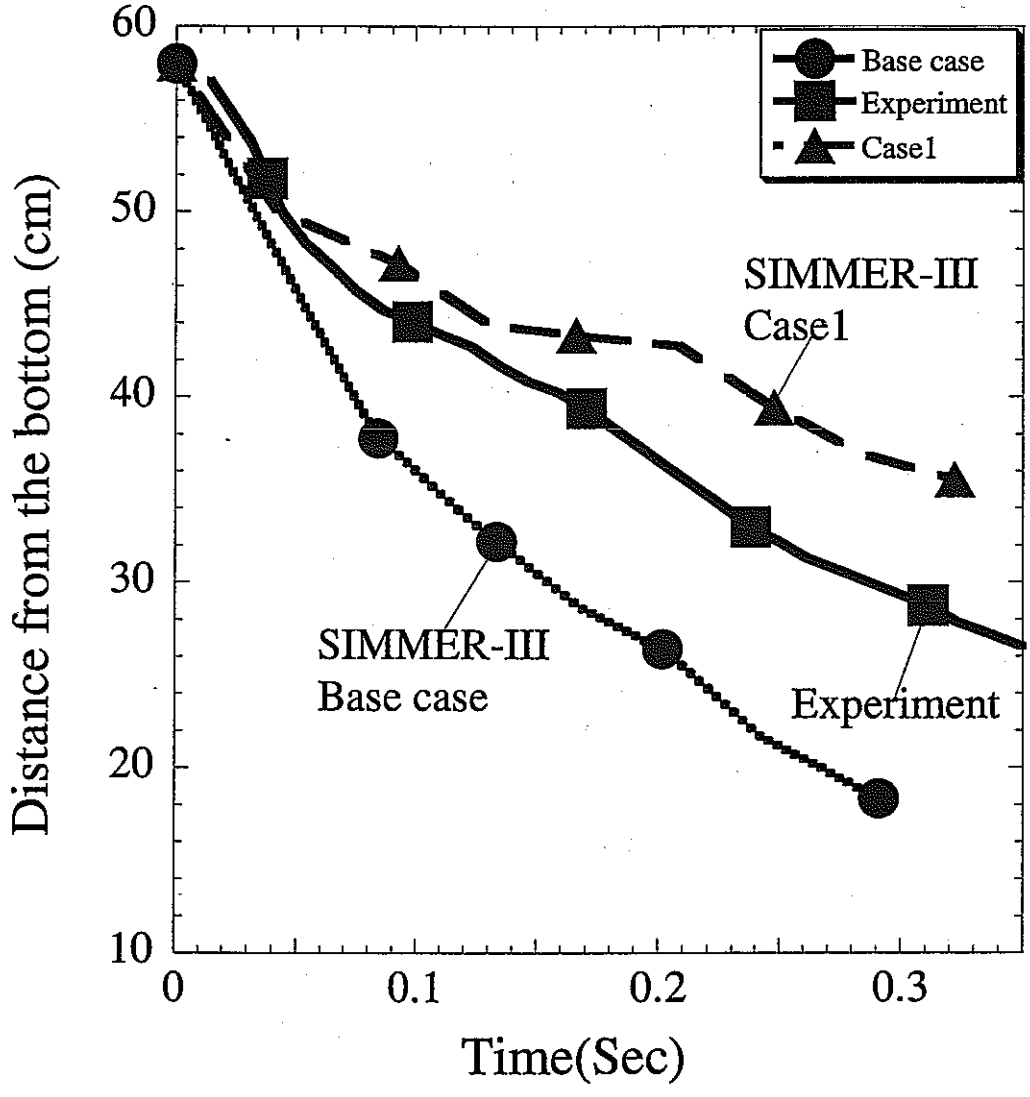

Fig. 8 Front advancement of the droplet stream in water in the experiment and the simulation (case1) of MIXA-06.

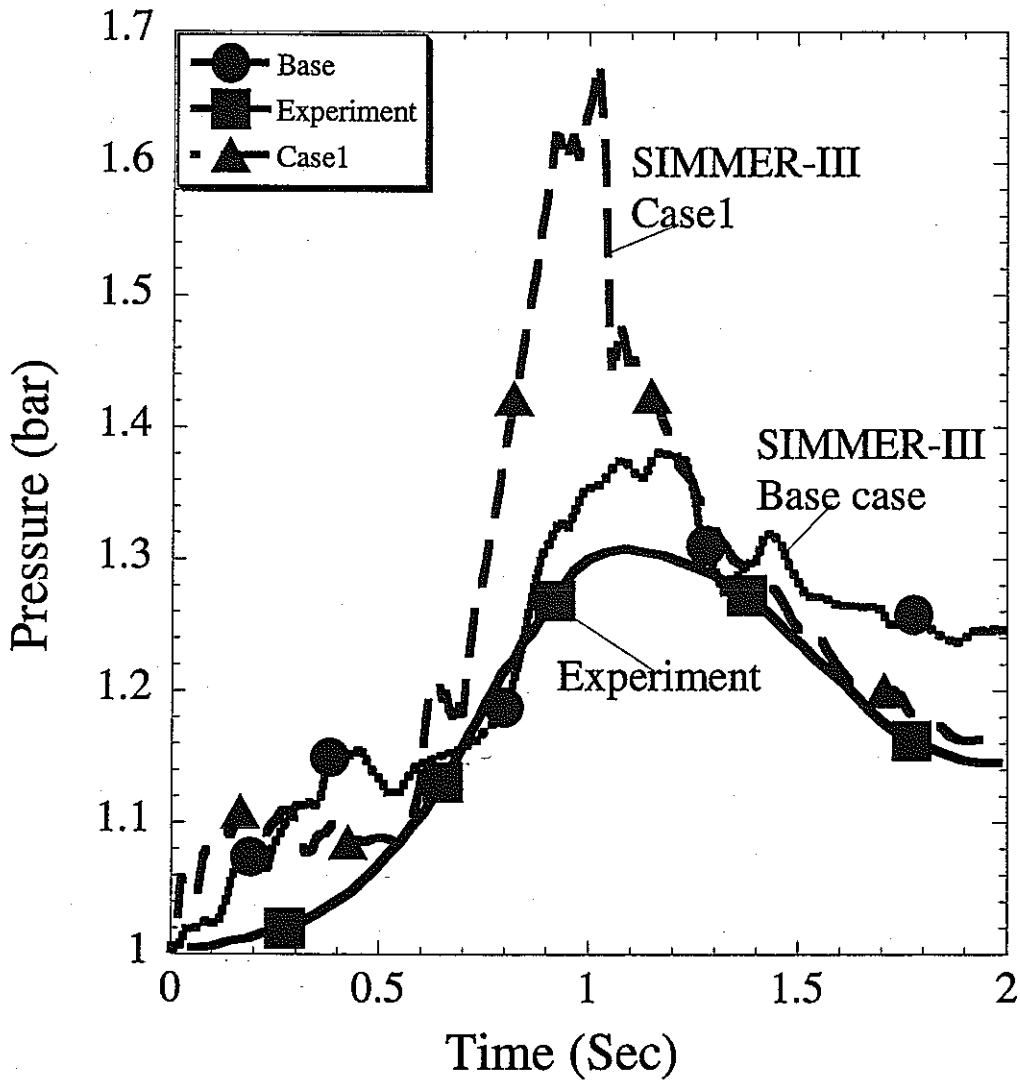

Fig. 9 The pressure transient in the free gas space in the experiment and the simulation (case1) of MIXA-06.

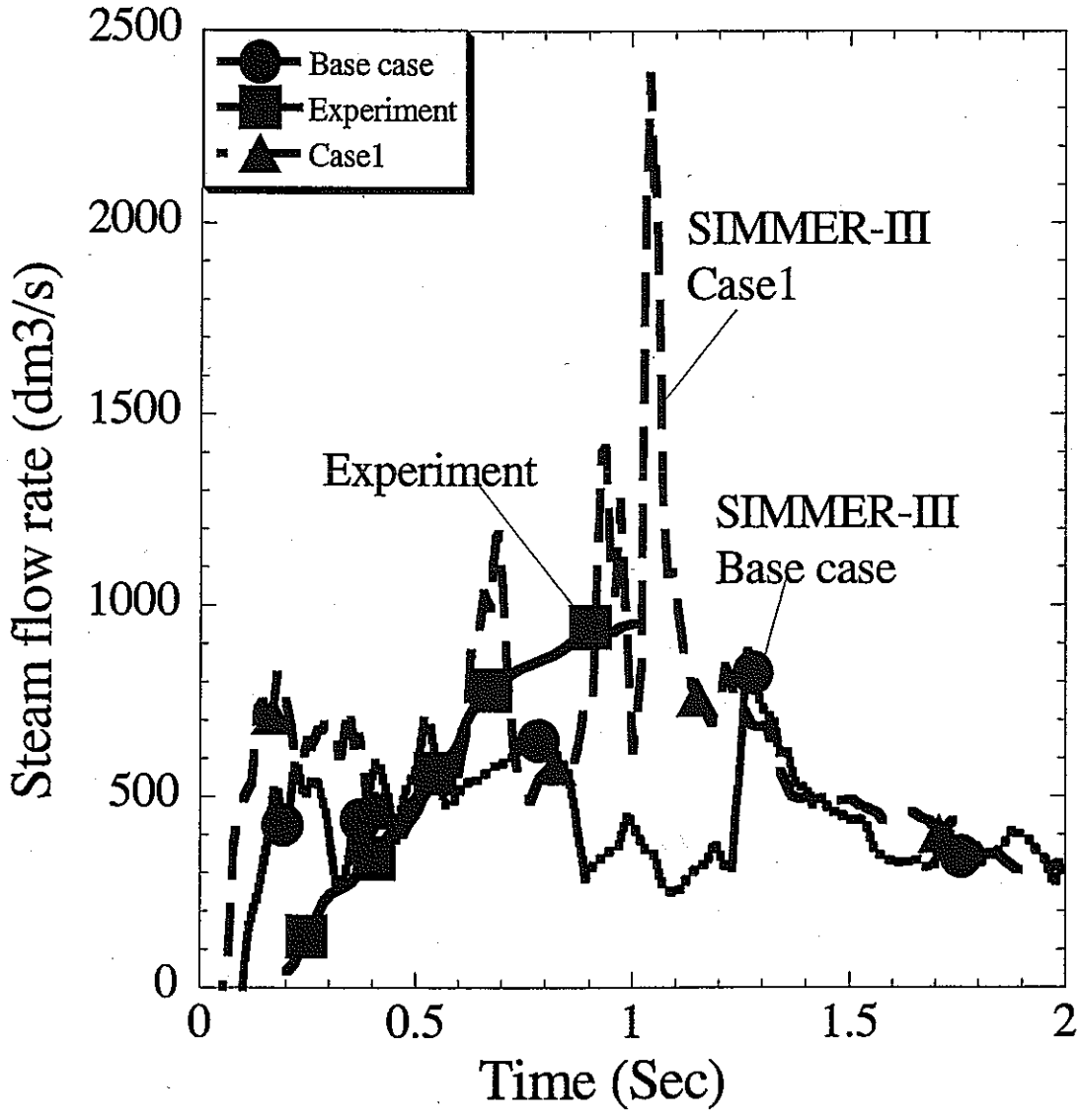

Fig. 10 Steam flow rate in the experiment and the simulation (case1) of MIXA-06.

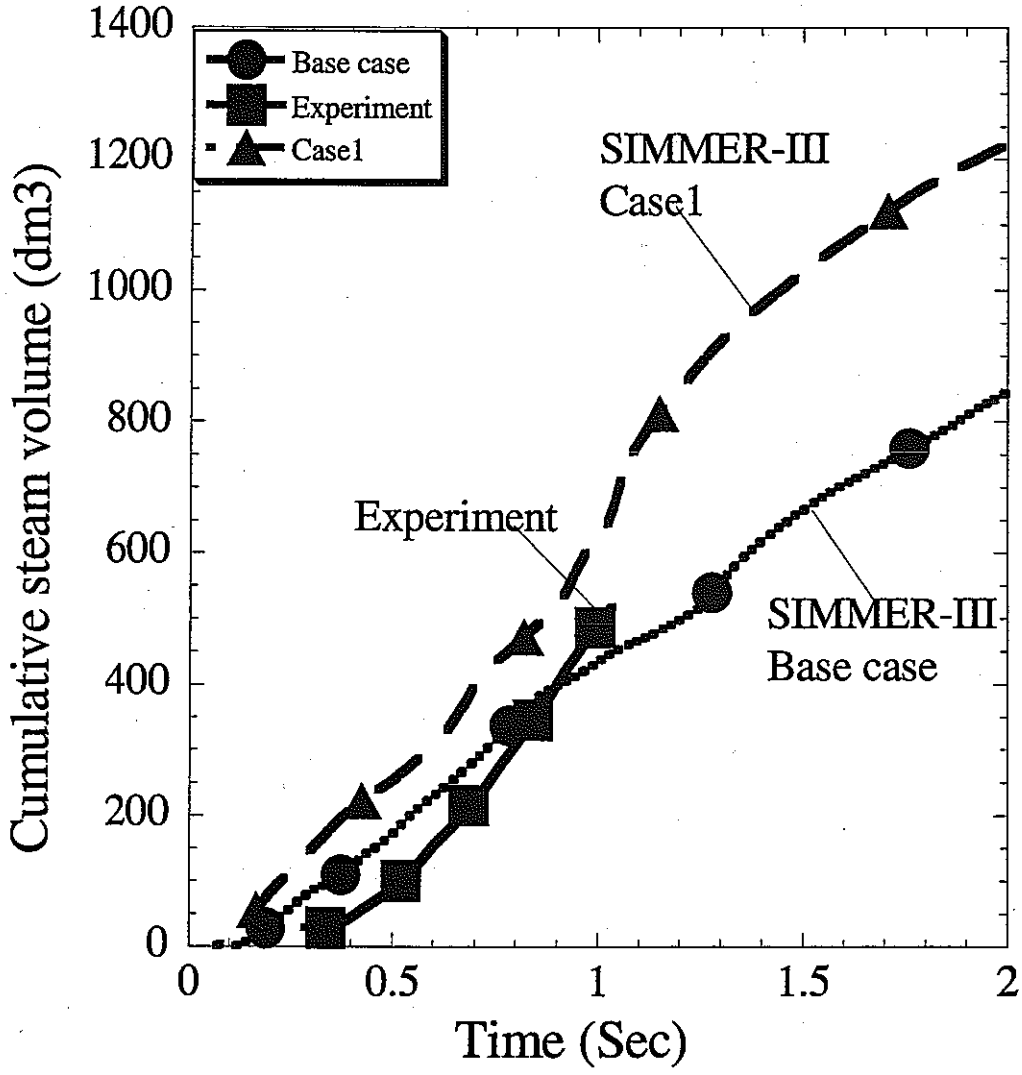

Fig. 11 Cumulative steam volume in the experiment and the simulation (case1) of MIXA-06.

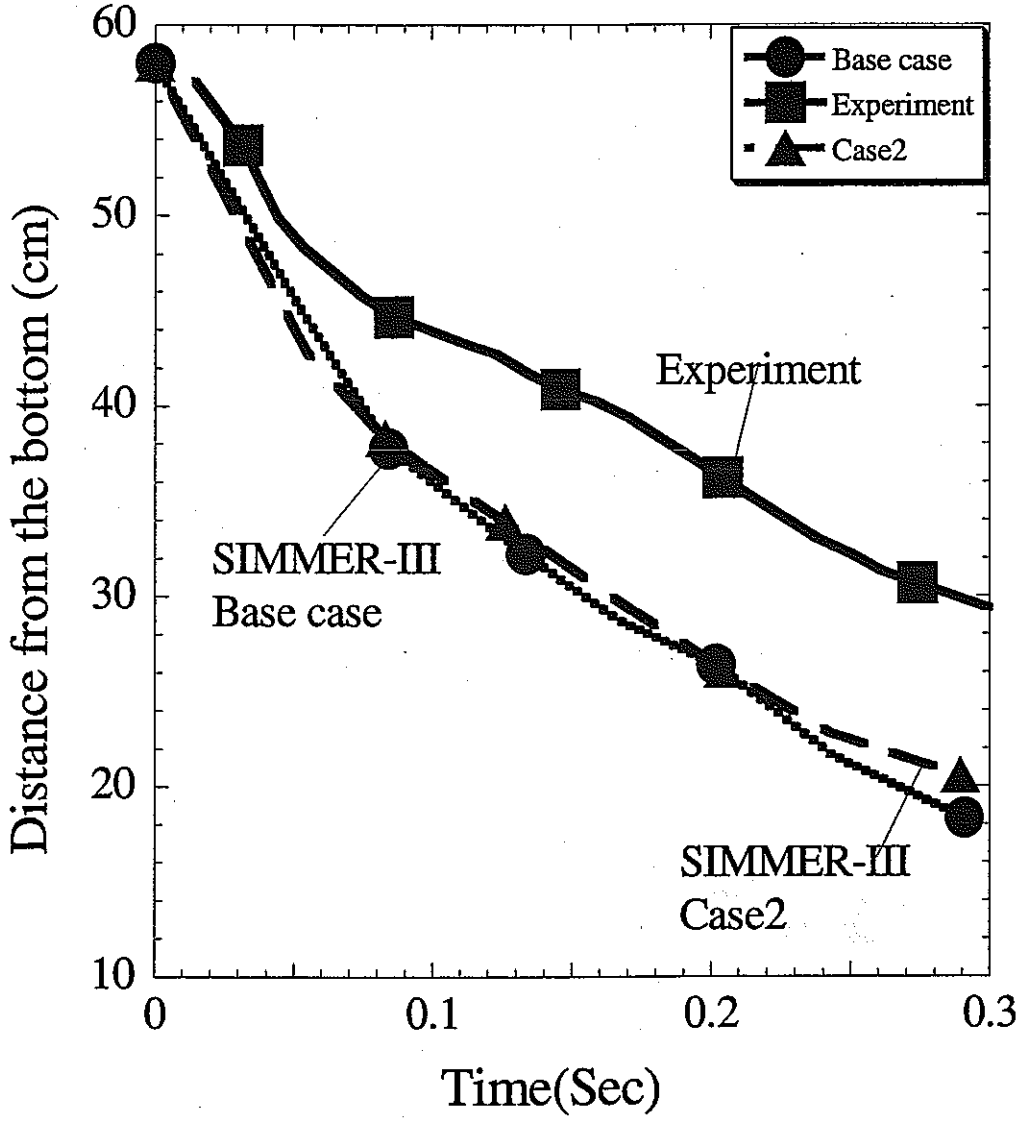

Fig. 12 Front advancement of the droplet stream in the simulation of MIXA-06 with different fragment size in Taylor fragmentation model.

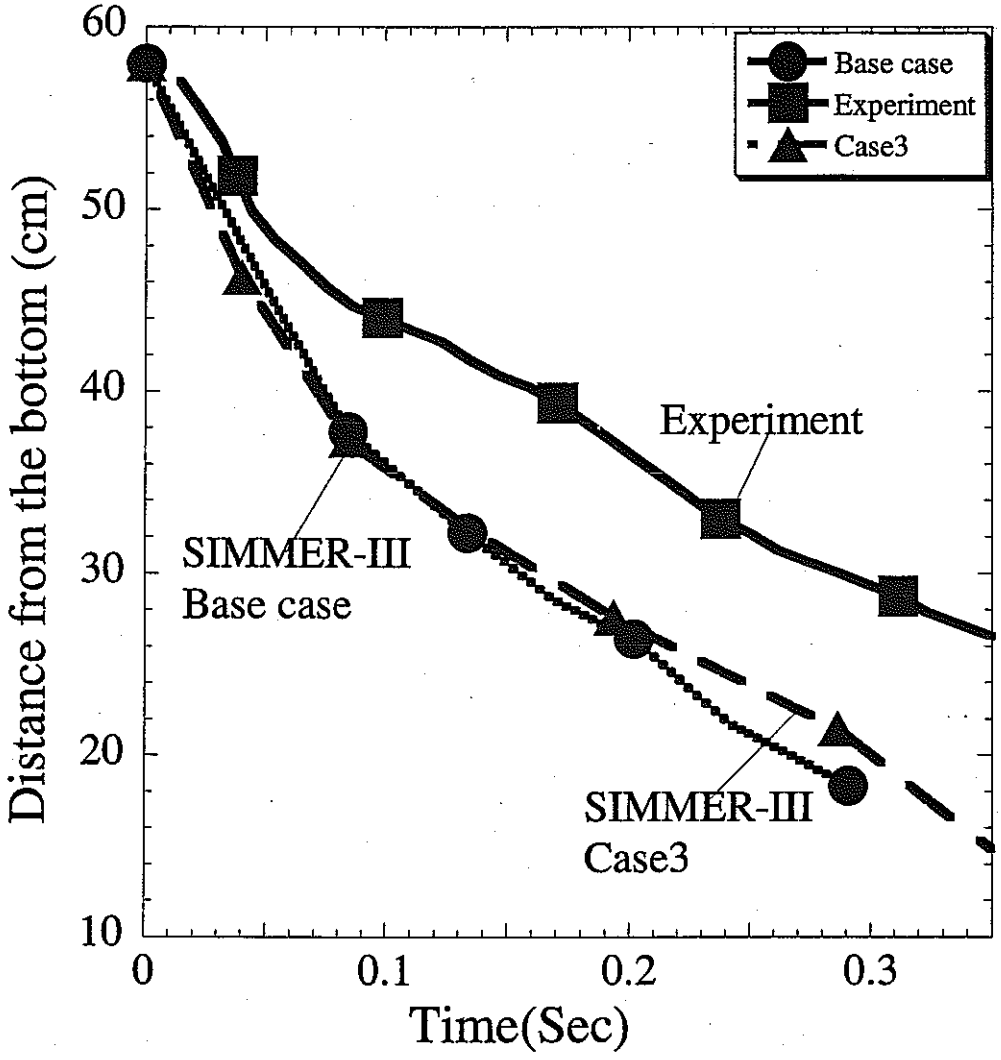

Fig. 13 Front advancement of the droplet stream in the simulation of MIXA-06 with different fragmentation time interval in Taylor correlation. Case3: fragmentation time is divided by 1000.

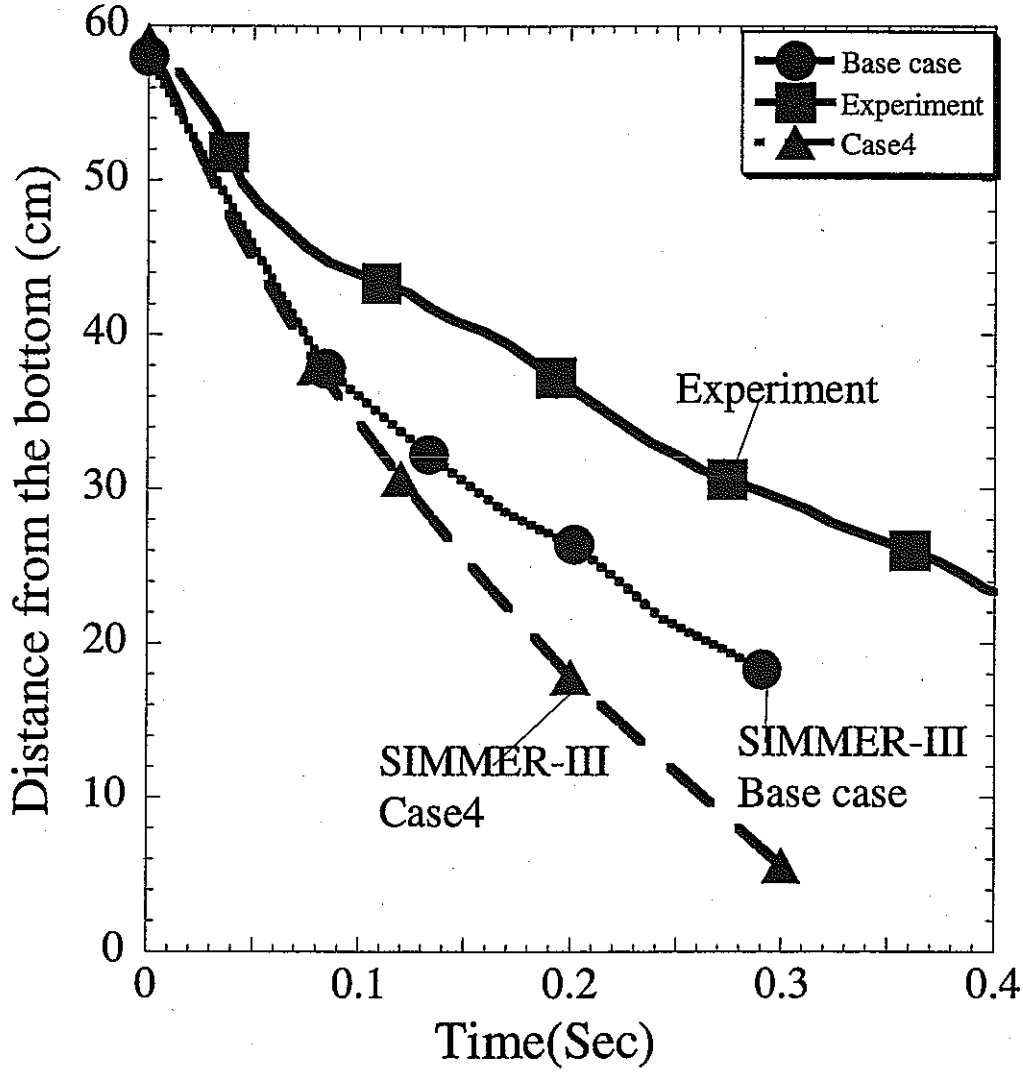

Fig. 14 Front advancement of the droplet stream in the simulation of MIXA-06 with different fragmentation models (1). Base case: Taylor correlation. Case4: no fragmentation.

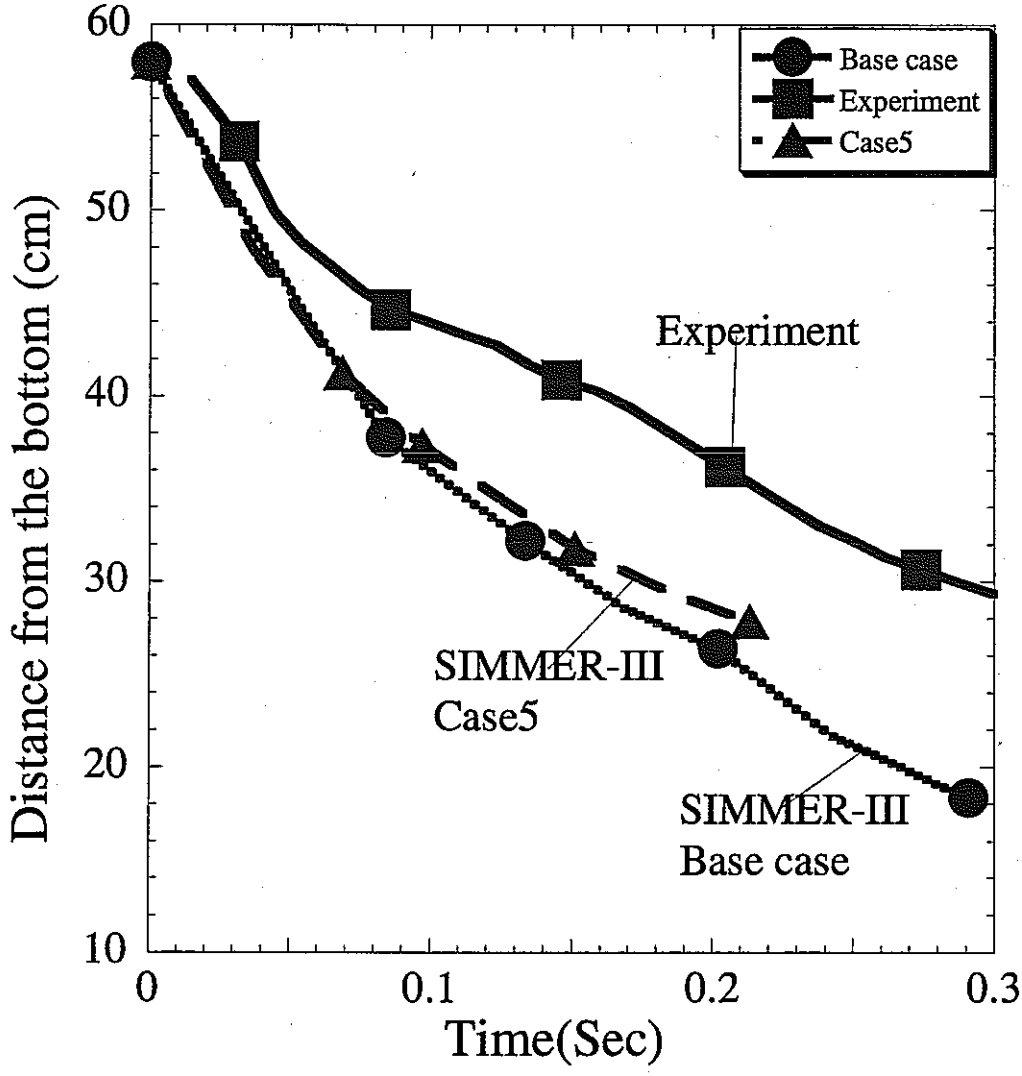

Fig. 15 Front advancement of the droplet stream in the simulation of MIXA-06 with different fragmentation models (2). Base case: Taylor correlation. Case5: Pilch_Erdman correlation.

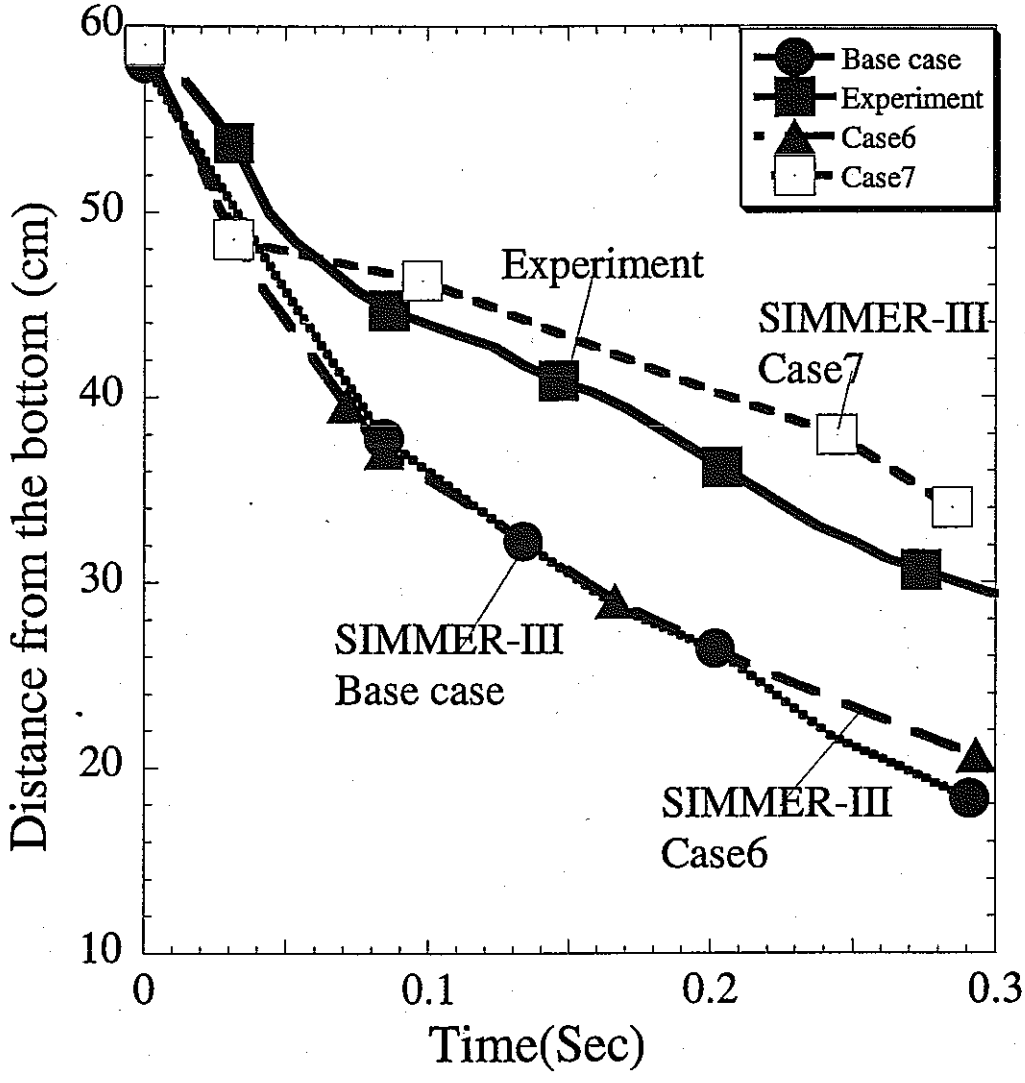

Fig. 16 Front advancement of the droplet stream in the simulation MIXA-06 with different fragmentation rate. Base case: CFSB, CFSD=1.0, Wecr=12. Base6: CFSB, CFSD=1.0, Wecr=0.12. Case7: CFSB, CFSD=0.001, Wecr=0.12.

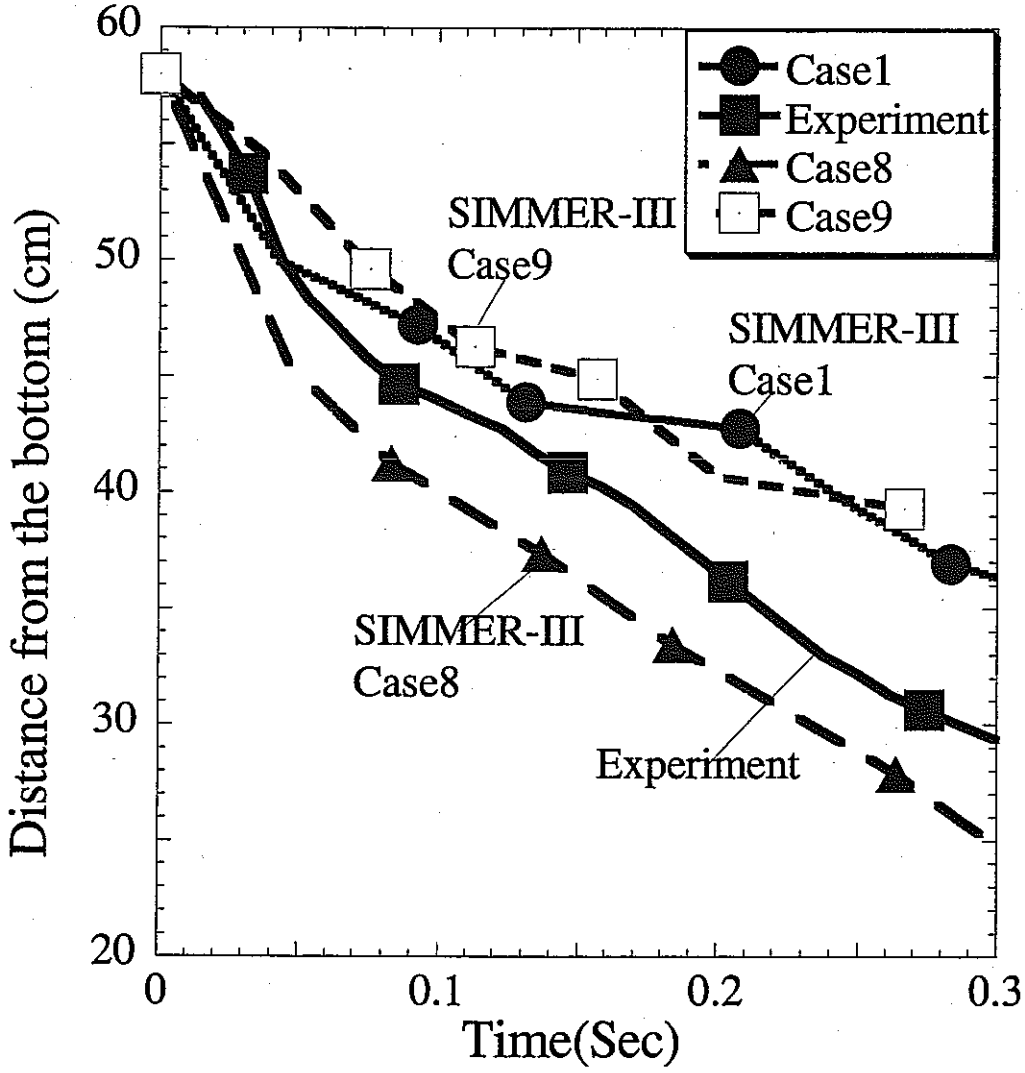

Fig. 17 Front advancement in the simulation of MIXA-06 with different fragment size. Case1: the radius of fragmented droplets is set to 0.001. Case8: the radius of fragmented droplets is set to 0.0015. Case9: the radius of fragmented droplets is set to 0.0007.

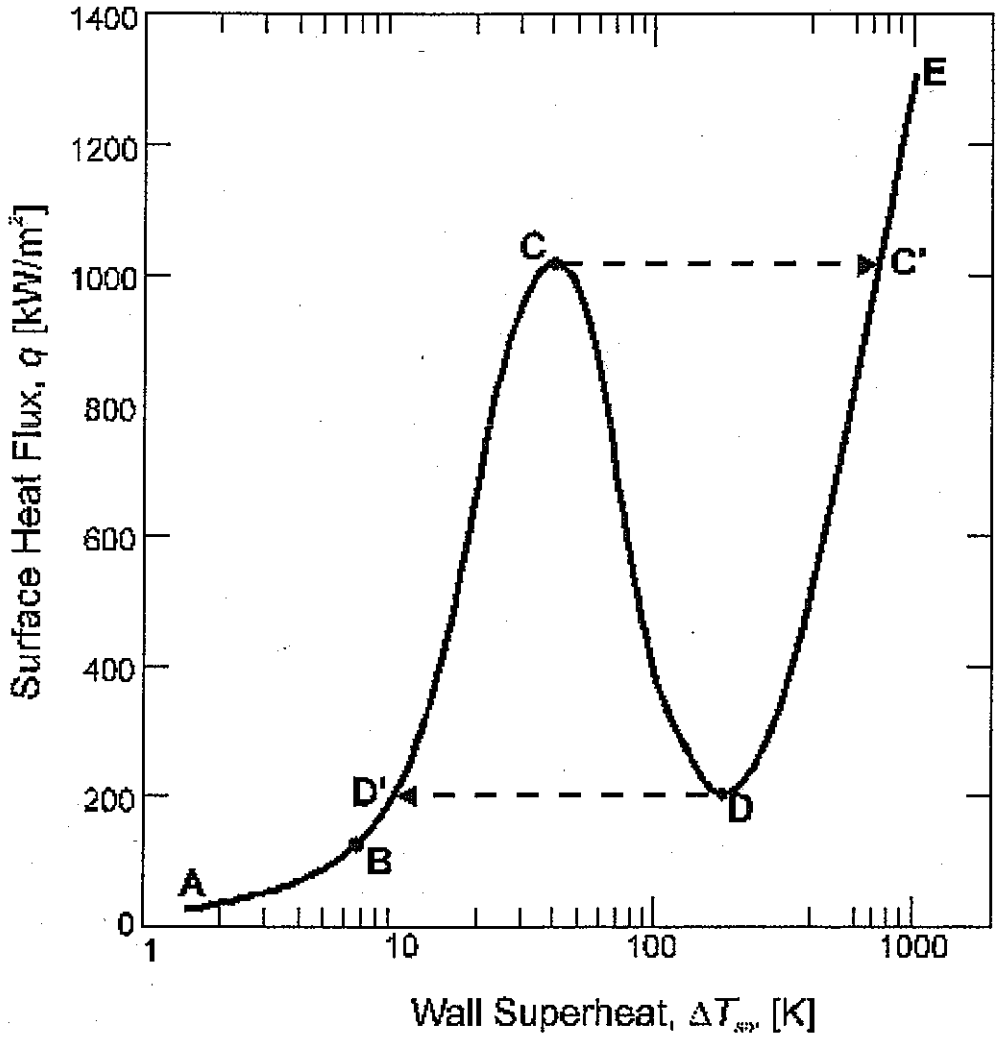

Fig. 18 Typical boiling curve for water at atmospheric pressure.

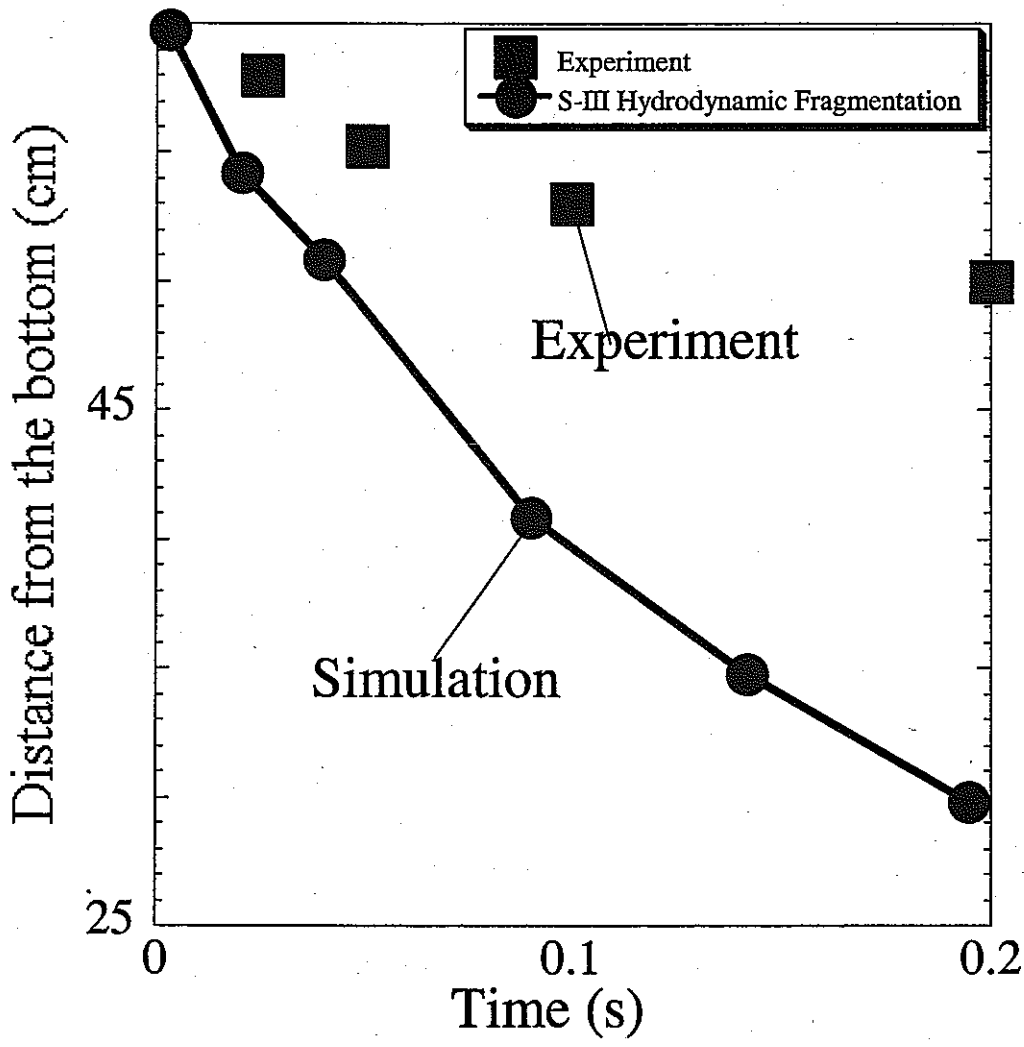

Fig. 19 Front advancement of the droplet stream in water in the experiment and the simulation (base case) of MIXA-01.

Appendix A Input Listing

```
      START: MIXA 06 ANALYSIS BY SIMMER-III
VER.2.F


      &XCNTL

       ALGOPT(1)    = 100*0,

       ALGOPT(1)    =      0,    0,    1,    1,    1,
0,    0,    0,    1,    1,

       ALGOPT(11)   =      1,    0,    0,    1,    1,
1,    1,    1,    1,    0,

       ALGOPT(24)   =      0,

       ALGOPT(31)   =      0,    0,    1,    0,    0,
0,    0,    0,    0,    0,

       ALGOPT(61)   =      0,    0,    0,    0,    1,
0,    0,    0,    0,    0,



       EOSOPT(1)    =      0,    0,    0,    0,    0,
0,    0,    0,    0,    0,



       HTCOPT(1)    = 100*0,

       HTCOPT(1)    =      0,    0,    1,    0,    0,
0,    0,    0,    0,    0,

       HTCOPT(7)    =      0,

       HTCOPT(10)   =      1,

       HTCOPT(11)   =      2,    0,    1,    1,    0,
0,    0,    0,    0,    0,



       IFAOPT(1)    = 100*0,

       IFAOPT(1)    =      1,    0,    0,    0,    0,
0,    0,    0,    0,    0,

       IFAOPT(20)   =      0,    0,    0,    0,    0,
0,    0,    0,    0,    0,



       HMTOPT(1)    = 100*0,

       HMTOPT(7)    =      51,

       HMTOPT(11)   =      0,    0,    0,    0,    0,
2,    0,    0,    0,    0,

       HMTOPT(51)   =      2,    2,

       HMTOPT(61)   =      1,


       EDTOPT(1)    = 100*0,

       EDTOPT(1)    =      1,    0,    0,    1,    0,
2,

       EDTOPT(11)   =      1,    0,    0,    0,    0,
0,    0,    0,    0,    0,



      &END


      &XMSH

       IB=10,JB=40,

       DRINP(1)=3*0.020,4*0.021,3*0.022,

       DZINP(1)=24*0.0375,    2*0.0375,    2*0.0375,
2*0.0375, 10*0.0375,

       NREG=3,

      &END


      &XTME

       TSTART       =     -0.38,

       TWFIN        =      2.00,

DTSTRT=4.0D-4,DTMIN=1.0D-06,DTMAX=4.0D-4,

       NDT0=1,TCPU=1000000.0,

      &END


      &XMSC

       COURTN       =     0.3,

       OPTPIT       =     9,

       MPIT         =     900,

       MAXITC       =     300,

       EPSVEL       =     1.0D-04,

       EPSP         =     1.0D+0,

       EPSRO        =     1.0D-04,

       EPST         =     1.0,

       EPSPCV       =     1.0D-04,
```

```
 IVDL(1)=1,1,2,1,1,2,3,
&END

&XERG
 REGC(1,1)=1,1,10,40,
 MATEOS(1,1)=2,1,2,1,2,
&END

        ### COVER GAS ###
&XRGN
LRGN=1,
 ILB=1,IUB=10,JLB=1,JUB=40,
 ALMINB(3)=1.0D-15,TLMINB(3)=371.0,
 ALMINB(1)=1.0D-15,
 PGMINB(3) = 1.0D+0,
 PG4INB    = 0.99999D+5,
 TGINB=371.0,
 TLMINB(3)=371.0,
 TLMINB(1)=3600.0,
 PGMINB(1) = 1.0000D-2,
 RLM0IB(1)=0.003,
 RGB0IB=0.001, XENRIB(1)=6*1.0,
 RGMINB=0.00005,
 RLM0IB(3)  =0.0001,  RLMINB(3)=0.000001,
RLMAXB(3)=0.0001,
 RLMINB(1)=0.001,RLMAXB(1)=0.003,
 RLMINB(4)=0.001,RLMAXB(4)=0.003,
&END

        ### Water POOL ###

&XRGN
LRGN=2,
 ILB=1,IUB=10,JLB=1,JUB=16,
 ALMINB(3)=1.000,TLMINB(3)=371.0,
 ALMINB(1)=1.0D-15,
 TLMINB(1)=3600.0,
 PSFINB=1.0D+05,TGINB=371.0,
 PGMINB(1) = 1.0000D-2,
 RLM0IB(1)=0.003,
 RGB0IB=0.001, XENRIB(1)=6*1.0,
 RGMINB=0.00005,
 RLM0IB(3)  =0.0001,  RLMINB(3)=0.000001,
RLMAXB(3)=0.0001,
 RLMINB(1)=0.001,RLMAXB(1)=0.003,
 RLMINB(4)=0.001,RLMAXB(4)=0.003,
&END

        ### Fuel ###
&XRGN
LRGN=3,
 ILB=1,IUB=3,JLB=40, JUB=40,
 ALMINB(3)=1.0D-15,TLMINB(3)=371.0,
 ALMINB(1)=0.055,
 TLMINB(1)=3600.0,
 PGMINB(1) = 1.0000D-2,
 TGINB     = 371.0,
 PGMINB(3) = 1.0000D+0,
 PG4INB    = 0.99999D+5,
 TGINB=371.0,
 RLM0IB(1)=0.003,
 RGB0IB=0.001, XENRIB(1)=6*1.0,
 RGMINB=0.00005,
 RLM0IB(3)  =0.0001,  RLMINB(3)=0.000001,
RLMAXB(3)=0.0001,
 RLMINB(1)=0.001,RLMAXB(1)=0.003,
 RLMINB(4)=0.001,RLMAXB(4)=0.003,
&END

&XBND
 NBC=0,
 LBCSET(1)=
```

```
      0,0,0,0,0,0,0,0,0,0,450*0,
      0,0,0,0,0,0,0,0,0,0,
      0,0,0,0,0,0,0,0,0,0,
      0,0,0,0,0,0,0,0,0,0,
      0,0,0,2,2,2,0,0,0,0,
      0,0,1,0,
    LWASET(3,40)=0100
    LWASET(3,39)=0100
    LWASET(3,38)=0100

   &END

   &XBND
    NBC      =  1,
    LBCS     =  2,
    LBCP     =  4,
    PTAB(1)  =  1.00D5, 1.00D5, 1.00D5, 1.00D5,
    PTME(1)  =  -0.500, 0.000, 0.5000, 4.0000,
   &END

   &XBND
    NBC      =  2,
    LBCS     =  3,
    LBCV(1)  =  6,6,6,
    VTAB(1,1) =  -0.72, -0.72, -0.72, 0.0, 0.0, 0.0,
    VTME(1,1) =  -10.43, -0.38, 0.62, 0.68, 1.0, 4.0,
    VTAB(1,2) =  0.0, 0.0, 0.0, 0.0, 0.0, 0.0,
    VTME(1,2) =  -10.43, -0.38, 0.62, 0.68, 1.0, 4.0,
    VTAB(1,3) =  -0.72, -0.72, -0.72, 0.0, 0.0, 0.0,
    VTME(1,3) =  -10.43, -0.38, 0.62, 0.68, 1.0, 4.0,
    LBCP     =  4,
    PTAB(1)  =  1.00D5, 1.00D5, 1.00D5, 1.00D5,
    PTME(1)  =  -0.500, 0.000, 0.5000, 4.0000,
   &END

   &XEDT
PRTC=999999,PPFC=999999,DMPC=999999,BSFC=500,
    NPRINT(1)=2,

    DTEOS(1,1)=3200,40,3600,
    DTEOS(1,2)=3200,40,3600,
    TCPPF(1)=22.0,120.0,
    DTPPF(1)=22.5,220.00165,
    DTPRT(1)=1.400,
    DTDMP(1)=1.998,

    NPAGE= 20,
    LPRGN(10)=1,1,1,1,1,
    LPRGN(16)=1,1,
    LPRGN(30)=0,1,1,1,0,1,1,0,0,0,
    LPRGN(70)=1,1,1,1,1,0,
    LPRGN(76)=1,
    LPRGN(96)=1,1,1, 1,1,1,
    SN(1)='ALPLK1','ALPLK2','ALPLK3',
'ALPLK4','ALPLK5','ALPLK6','ALPGK','ALPGE','PK','IRGMK',
'TLK1','TLK2','TLK3','TLK4','TLK5','TLK6','TGK',
        'EIPINK','SIEGK',
'SIELK1','SIELK2','SIELK3','SIELK4','SIELK5','SIELK6',
```

```
'VK1','VK2','VK3','UK1','UK2','UK3','TIPINK','ALPINK',

'ALPNFK1','ALPNFK2','ALPNFK3','RGBK','CPK','DPK',
        'QN1','QN2','QN3','QN4','QN5',

'RBGK1','RBGK2','RBGK3','RBGK4','RBGK5',

'RBLK1','RBLK2','RBLK3','RBLK4','RBLK5','RBLK6','RBLK7','RBLK8',
        'RBLK9','RBLK10',
        'RBIK1','RBIK2','RPINK','DHK',

'RLMBK1','RLMBK2','RLMBK3','RLMBK4','RLMBK5',

'RLMDK1','RLMDK2','RLMDK3','RLMDK4','RLMDK5',
        'RGBK',
        'ALPGEK','ASMZ',
        'TSAT1','TSAT2','TSAT3',
        'PGMK1','PGMK2','PGMK3','PGMK4',
        'AQSTK1','AQSTK2','BQSTK1','BQSTK2',
 &END
 &XIFA
  DHPOOL= 1.0,
 &END
 &XHTC
  HFCLP(1,3) =  5.10000D-01,
  HFCLP(2,3) =  5.00000D-01,
  HFCLP(3,3) =  4.00000D-01,
  HFCLP(4,3) =  1.50000D-02,
  HFCLP(5,3) =  3.33333D-01,
  HNCLP(1,3) =  5.00000D-01,
  HNCLP(2,3) =  2.50000D-01,
  HNCLP(3,3) =  1.18000D-00,
  HFCLS(1,3) =  2.30000D-02,
  HFCLS(2,3) =  8.00000D-01,
  HFCLS(3,3) =  3.00000D-01,
  FILMIN     =  1.00000D-04,
  CMFB       =  0.64,
  HCDGS      =  5.0,
  HCDLAS(1)  =  3*2.0,
 &END

 &XHMT
  PHI   = 0.01,
  FTSTL = 0.6,
  FTSTH = 0.95,
 &END

 &XMXF
  FCOUPL = 1.0D-8,
  CDD = 1.00,
  CCD = 1.00,
  CORFZN(10,40) =1.0,
 &END
```